THE EFFECT OF DIFFERENT CURING METHODS ON ELECTRICAL PROPERTIES OF CONCRETE

By

RAID S. ALRASHIDI

A THESIS PRESENTED TO THE GRADUATE SCHOOL
OF THE UNIVERSITY OF FLORIDA IN PARTIAL FULFILLMENT
OF THE REQUIREMENTS FOR THE DEGREE OF
MASTER OF SCIENCE

UNIVERSITY OF FLORIDA

2018

To my lovely family and to my best friends, Waleef and Majeed

ACKNOWLEDGMENTS

First and foremost, I am very grateful to God Almighty for his graces, blessing, and protection over my life, and for giving me strength and the ability to successfully complete this research.

I would like to express my deepest gratitude for my advisor Dr. Kyle A. Riding for his extraordinary help, guidance, and motivation throughout my graduate education. He has not just made me a better engineer, but made me a successful person. Appreciation is also extended to Dr. Mang Tia, and Dr. Christopher Ferraro for serving on my supervisory committee.

I would also like to thank all my labmates and friends. Special thanks go to Abdulmajjid Alrashidy, Mohammed Almarshoud, Hossein Mosavi, Mohammed Hussain Alyami, Waleed Almasoud, and Nader Aljohani for all the support, advice, and help they have provided me. They have also helped me sustain a positive atmosphere in which to complete this work.

Finally, I am also grateful and indebted to my beloved family for their unconditional love and constant support for my whole life. Without all the help and encouragement from faculty, friends, and family, this work would not have been possible.

TABLE OF CONTENTS

LIST OF TABLES

LIST OF FIGURES

LIST OF ABBREVIATIONS

C-100	100 % type I/II cement with low w/cm (0.35)
C-100h	100 % type I/II cement with high w/cm (0.44)
CL-F20S8	Type L cement with a 20% of fly ash and 8% of silica fume
CV-F10G60	Type V cement with a 10% of fly ash and 60% of slag cement
F	Formation factor
FA	Fly ash
G	Slag
HA cement	High Alkali cement
M	Metakaolin
RCPT	Rapid chloride permeability test
S	Silica fume
SCMs	Supplementary cementitious materials
W/cm	Water to cementitious materials ratio

Abstract of Master Presented to the Graduate School
of the University of Florida in Partial Fulfillment of the
Requirements for the Degree of Master of Science

THE EFFECT OF DIFFERENT CURING METHODS ON ELECTRICAL PROPERTIES OF CONCRETE

By

Raid S. Alrashidi

August 2018

Chair: Kyle A. Riding
Major: Civil Engineering

Electrical measurements have become a popular method of assessing the transport properties of concrete because they are rapid, easy to perform, and low cost. Even though these measurements can be easily obtained, many factors can affect the results obtained such as specimen geometry, degree of saturation, temperature, pore solution composition, and curing method. There is a concern that standard moist-room curing may cause leaching, affecting the results. Thirty-eight different concrete mixtures were made and cured using two different methods to determine if curing samples in a simulated pore solution would reduce leaching and give more reliable results. Mixtures were made with different types of cement, fly ash, silica fume, slag, and metakaolin. Binary and ternary blends were used. It was found that bulk resistivity showed less issues with ion migration than surface resistivity measurements. It was also found that while curing samples in a simulated pore solution could reduce significantly leaching, surface resistivity measurements gave unreliable measurements in some cases.

CHAPTER 1
INTRODUCTION

1.1 Background

Concrete electrical property measurement as a quality control tool has been ongoing for several decades (Sohn & Mason, 1998)(Rupnow & Icenogle, 2012) . These tests use the electrical resistance as an indicator of the water and ionic penetrability of the concrete. Electricity is conducted through the concrete principally by the pore solution in the concrete pores. The higher the volume and connectivity of the pores, the higher the electrical conductivity of the concrete.

A technique has been developed recently to measure the concrete resistivity non-destructively. This technique uses a four-probe Wenner probe to measure the concrete surface resistivity or bulk resistivity. Electrical resistivity tests such as surface and bulk resistivity have become used by the Florida Department of Transportation (FDOT), and the Louisiana Department of Transportation (LADOT) because of their simplicity. FDOT has recently become concerned that these tests do not sufficiently measure the concrete's resistance to chloride ion penetration when more than one type of supplementary cementitious materials (SCMs) is used. SCM use change the pore solution composition and corresponding electrical resistivity. The change in pore structure refinement rate caused by the different hydration rate of SCMs could affect the rate of leaching out of ions from the concrete during curing. Changes to the curing process could eliminate this issue. Normalization of the concrete electrical resistivity by the pore solution resistivity could account for some of the differences seen.

1.2 Hypothesis of Research

Curing concrete samples in a simulated pore solution can eliminate leaching and lead to more reliable electrical resistivity results.

1.3 Research Objectives

The main objectives of this research project as follows:

- To measure the effect of using simulated pore solution to cure concrete on surface and bulk resistivity measurements.

- To measure the effect of SCMs as well as the w/cm on the electrical properties of concrete with time.

1.4 Scope of the Research

Thirty-eight mixes with a two w/cm ratio of 0.35 and 0.44 were performed including four different types of cement, I/II, V, L, and high alkali cement, and four SCMs, fly ash, slag, silica fume, and metakaolin were used for this research project. The surface resistivity and bulk resistivity of the concrete mixtures were measured according to AASHTO T 358 and AASHTO TP 119, respectively. Measurements were made at 28, 56, and 91 days after mixing. Samples were made for curing in the moist room and simulated pore solution for comparison.

CHAPTER 2
LITERATURE REVIEW

2.1 Introduction

Concrete is the most widely used building material in the world in part due to its favorable durability-to-cost ratio. Durability of concrete is substantially enhanced by the incorporation of supplementary cementitious materials (SCMs). Many SCMs are industrial byproduct that reduce the concrete greenhouse gas footprint (Scott & Alexander, 2016)(Borosnyói, 2016). In general, SCMs such as fly ash, silica fume, slag cement, and metakaolin can enhance strength and durability by acting hydraulically or pozzolanicly. The term hydraulic describes the material that chemically reacts with water to form a stable product under water, such as portland cement and slag cement. The term pozzolanic is a description given to a material, primarily siliceous in composition, when reacts with water, displays little cementitious properties, such as Class F fly ash, and silica fume. SCMs contribute to the hydration of portland cement by physical phenomena and by chemical reaction. Due to pozzolanic activity and the filler effect, SCMs can enhance concrete mechanical properties and reduce the concrete penetrability (Borosnyói, 2016)(Chini, Muszynski, & Hicks, 2003).

Electrical resistivity test methods have been developed to help measure the concrete resistance to fluid and ion transport. Interpretation of electrical resistivity test results for concrete durability requires an understanding of both the materials tested and the test mechanism and methods used. This literature review provides an in-depth examination of typical SCMs and electrical test methods used in concrete.

2.2 Fly Ash

Fly Ash (FA) is a pozzolanic material that is a by-product of coal combustion for the generation of electricity. Most fly ash particles are amorphous, spherical and small in size, ranging between 1.0 and 100 μm in diameter. In the United States, fly ashes for use in concrete are categorized as Class F and Class C as described in ASTM C618. Classification is based on their chemical composition that depends on the type of coal burned, in which the sum of SiO2, Al2O3, and Fe2O3 should be greater than 70% for Class F fly ash, and greater than 50% for Class C fly ash (ASTM, 2010a). Although not a requirement in the standard, a primary difference between the Class F and Class C ashes is the amount of calcium oxide (CaO). Class C has much higher calcium content than Class F, and can have high variability of the chemical composition (Ponikiewski & Gołaszewski, 2014)(Yamei, Wei, & Lianfei, 1997).

The spherical nature of fly ash particles is often improve concrete workability. (Khan, Nuruddin, Ayub, & Shafiq, 2014). Concrete workability is affected by high carbon content, in which the porous carbon particles absorb more water (Neville, 2011). As a negative side effect of fly ash, it has been reported that higher dosages of air entrainment are required due to its adsorption to the surface of unburned carbon particles (Jolicoeur et al., 2009). Class F fly ash is also known to lower the amount of heat hydration, which makes it very useful in mass concrete application. Class C fly ash, however, it depends on its chemical composition and can either increases or decreases the heat of hydration. Incorporation of class F fly ash can low early compressive strength; however, due its pozzolanic reaction, the later strength gradually improves over time (Saha, 2018). Class F fly ash can increase the sulfate resistance due to the continued reaction with hydroxides , whereas Class C fly ash mixture have a greater

susceptibility to reduce sulfate resistance (ACI, 2002). With respect to Alkali Silica Reaction (ASR), the use of adequate amounts of fly ashes can mitigate ASR expansion by reducing hydroxyl ions in pore water and consuming CH. However, class C fly ash may require a higher dosage than Class F fly ash to mitigate ASR because of its high chemical variability, and lower alkali binding.

The use of fly ash as a partial replacement of portland cement is common. Using fly ash as an SCM can greatly improve the sulfate resistance and the chloride permeability (X. Shi, Xie, Fortune, & Gong, 2012)(J. Su et.al., 2002). The combined use of fly ash with other SCMs, such as slag, whether in small or large cement substitution ratio can lead to a favorable durability performance of concrete (Ganesh Babu & Sree Rama Kumar, 2000)(Xu, 1997). The presence of fly ash can lower the alkali and hydroxide concentration in the pore solution (Vollpracht, Lothenbach, Snellings, & Haufe, 2016). The reactivity of SCMs such as fly ash is influenced by the alkalinity of pore solution of concrete. When fly ash is used as a partial replacement with cement, the alkali (potassium and sodium) concentrations decrease with time and result in the formation of C-S-H with a lower Ca/Si ratio and alkali binding (Vollpracht et al., 2016). The pozzolanic reaction leads to C-A-S-H phases., At longer hydration times, the concentration of hydroxides are also decreased (Hong & Glasser, 1999)(Vollpracht et al., 2016)

2.3 Slag Cement

Slag cement is highly cementitious in nature, and it is a by-product of the process of making steel in a blast furnace. Molten slag is rapidly quenched whether in air or water to form glassy granules, which are then ground. Faster quenching, higher temperatures rates and higher alkali content can make the slag more reactive. Slag

cement particle fineness and specific area is similar to portland cement particles, and has a very limited amount of crystalline material (Hadj-Sadok, Kenai, Courard, & Darimont, 2011). In accordance with ASTM C989, based on the activity index, the slag is divided into three grades: grade 80, 100, and 120, in which the higher grade contributes more to the compressive strength at 7 and 28 days (ASTM, 2013a). The sulfur in sulfide form in slag cement must not exceed the allowed limit, 2.5 % (ASTM, 2013a).

The initial reaction of slag is often relatively slow; therefore, setting time can be increased compared to portland cement. Slag cement reactivity is highly temperature dependent. Use of slag cement in cold-weather may require heating or use of an accelerator since it hydrates very slow at low temperature. It has reported that replacing large percentages of portland cement with slag can lower the heat of hydration (Neville, 2011). The addition of slag up to 55% resulted in improved concrete workability as well as increased bleed capacity (by 30% compared to the control) with little effect on the bleeding rate (Wainwright & Rey, 2000). The reactivity of slag can influence the strength development of concrete, and incorporation of slag up to 60% can lower the compressive strength at early ages, but lead to a comparable later age compressive strength (Malagavelli, 2010a). Slag cement is effective in mitigating alkali silica reaction ASR, in which it consumes CH and binds alkalis in C-S-H reaction.

With addition of slag, the concrete's resistance to sulfate and chloride attack is increased (Malagavelli, 2010b). Slag improves the durability considerably of portland cement concrete exposed to chloride environments by improving the pore structure of

concrete and increasing the material chloride binding capacity (Luo, Cai, Wang, & Huang, 2003)(Cheng, Huang, Wu, & Chen, 2005).

The slag proportion in cement can affect the alkali concentration, however, if the alkali level in both slag and clinker are similar, the reactivity of the slag doesn't highly affect the alkalinity concentration of the pore solution (Chen & Brouwers, 2011). Since slag cement contains less alkali compared to the normal portland cement, it lower the potassium and sodium concentrations and reduces sulfur species, thus decreases the OH- concentrations of the pore solution (Vollpracht et al., 2016).

2.4 Silica Fume

Silica fume (SF) is a pozzolanic material that is by-product of the silicon and ferrosilicon industry. Most SF particles are made up mostly of amorphous silica (SiO_2 >85%) and are very small in size, typically averaging from 0.1 and 0.5 μm in diameter. Silica fume acceptance is governed by ASTM C1240 (ASTM, 2012). Due to its high fineness, it reacts much faster than fly ash and slag, and may increase the water demand of concrete; therefore, it is usually accompanied with the use of superplasticizer. The high reactivity of SF can lead to a significant increase in the compressive strength. SF is also known at mitigating ASR due to the reduction in pore solution alkalinity, therefore when it used in sufficient amounts, the expansion may be decreased to harmless level (Press & May, 1992). SF in modest quantities (3-5%) can considerably reduce the penetrability of concrete as it changes the microstructure through both chemical and physical pathways. Spoge et.al., (Song, Pack, Nam, Jang, & Saraswathy, 2010) verified a microstructure model for SF cement concrete and concluded that incorporating up to 8% silica fume in the concrete makes the microstructure of the concrete denser and significantly reduces the permeability. SF

reduces the connectivity and size of the pores due to the growth of the secondary C-S-H and consumption of calcium hydroxide (Hassan, 2001). Partial replacement of the portland cement with silica fume is known to reduce the C/S ratio of the C-S-H. This can reduce the chloride binding slightly by reducing the amount of chloride that adsorbs onto the surface of C-S-H. The presence of SF decreases the alkali and hydroxide level in the pore solution and becomes more distinct with time when more SF reacts (Vollpracht et al., 2016). Compared to the control mix, a partial cement replacement of 5% by silica fume decreases the pore solution conductivity by 75% during the first 7 days (C. Shi, 2004). The incorporation of silica fume reduces the pH of the pore solution of concrete and increases the amount of C-S-H formed (M. D. A. Thomas, Hooton, Scott, & Zibara, 2012).(M. D. A. Thomas et al., 2012). Silica fume decreases the alkali and hydroxide concentrations in the pore solution more than fly ash due to the higher reaction degree of the silica fume and higher silicon content, in which the reaction is much stronger than for fly ash.(Vollpracht et al., 2016).

2.5 Metakaolin

Metakaolin (MK) is a processed kaolin clay that is calcined between 500 and 800 ℃ to create an amorphous aluminsolicate SCM. The particle size of MK is finer that the portland cement particle. It is a highly reactive aluminosilicate pozzolan that combines with calcium hydroxide to produce additional calcium silicate hydrates (C-S-H), aluminosilicate hydrates (C-A-S-H), and aluminate hydrates (C-A-H) (Ramezanianpour & Bahrami Jovein, 2012) . MK can significantly reduce the workability of concrete (Frías, De Rojas, & Cabrera, 2000). MK has a high silicon dioxide (SiO2) and alumina (Al2O3) content of 51.52% and 40.18% by mass, respectively. The high alumina content makes it very effective in mitigating delayed ettringite formation (DEF)

(Ambroise, Maximilien, & Pera, 1994)(A. Santos Silva, 2015). The use of MK as a partial replacement of portland cement can increase the compressive strength; however, it is found that when the mix contains both metakaolin and silica fume, the higher the MK dosage, the less the increase in the compressive strength (Borosnyói, 2016). The incorporation of MK in concrete can significantly increase its resistance to the chloride penetration by decreasing the mean pore size (Ramezanianpour & Bahrami Jovein, 2012)(Y.Liu, 2012). The pozzolanic reaction of the metakaolin was found to consume portlandite and produce a more refined pore system (Justice & Kurtis, 2007). When using MK with concrete, the surface electrical resistance of concrete was greatly enhanced compared to the reference concrete, giving 2-4 times higher resistivity for a 15% MK dosage (Ramezanianpour & Bahrami Jovein, 2012)(Borosnyói, 2016). MK modifies the pore structure and substantially lowers the permeability of concrete resulting in increased resistance to diffusion of chloride ions and the transportation of water (Siddique & Klaus, 2009).

2.6 Pore System and Formation Factor

Over the last several decades, a lot of has focused on the electrical properties of concrete as a concrete quality indicator. Electrically conductive pore solution can fill concrete pores, making the concrete electrically conductive. The electrical conductivity of the concrete is dependent on both the pore system and the pore solution conductivity. The concrete electrical resistivity ρ_T (Ω.m), or inverse of conductivity, can be normalized by the pore solution resistivity ρ_0 (Ω.m) to give an empirical material pore system index called the Formation Factor (*F)*, as shown in Equation 2-1 (Kenneth A. Snyder, 2001):

$$\frac{\rho_T}{\rho_0} = F \tag{2-1}$$

F is independent of specimen size or shape and is related to the pore system as the inverse of the product of the concrete porosity volume Ø and connectivity β, as shown in Equation 2-2 (Archie, 1942)(R. Spragg, Bu, Snyder, Bentz, & Weiss, 2013)(Spragg, 2013):

$$F = \frac{1}{\emptyset\beta} \tag{2-2}$$

The Nernst-Einstein relationship can also be used to relate F and the concrete electrical resistivity to the concrete bulk effective diffusion coefficient D (m^2/s), as shown in Equation 2-3: (Bu & Weiss, 2014)(Kenneth A. Snyder, 2001).

$$\frac{\rho_T}{\rho_0} = F = \frac{D_o}{D} \tag{2-3}$$

Where D_0 is the self-diffusion coefficient (m^2/s). Equation 2-2 shows how the concrete resistance against chloride penetration can be proportional to the concrete electrical properties. This relationship is what allows concrete electrical tests to be used for concrete quality tests.

The concrete pore system, pore solution conductivity and consequently electrical resistivity are highly dependent on the concrete mixture characteristics such as cementitious material composition, water-to-binder ratio, and degree of hydration (R. Spragg, Bu, et al., 2013). As the concrete hydrates with time, the microstructure and pore solution can also be significantly changed due to environmental conditions (R. Spragg, Bu, et al., 2013)(Spragg, 2013). Temperature, leaching of alkalis, and degree of

saturation can all affect pore solution composition and electrical resistivity measurements.

The pore solution resistivity can be estimated using the NIST pore solution electrical conductivity calculator (based on the mixture proportion and the alkali content), which is available online http://concrete.nist.gov/poresolncalc.html, experimentally by using embedded sensor into a fresh concrete (Rajabipour, Sant, & Weiss, 2007) or from pore solution extraction (Barneyback, Diamond, 1981).

2.7 Electrical Resistivity and Conductivity Tests

Over the last few decades, different methods have been suggested to measure the electrical properties of concrete. (W.J. Weiss, J.D. Shane, A. Mieses, T.O. Mason, S.P. Shah, 1999)(J. Calleja, 1952). The first concrete electrical test method developed is the rapid chloride permeability test (RCPT), standardized as ASTM C1202 (ASTM C1202, 2012) or AASHTO T277 AASHTO T277 standards. Although this test has gained wide use, it is a destructive test, requires a significant amount of sample preparation, and has other shortcomings that cause issues with repeatability (Riding, Poole, Schindler, Juenger, & Folliard, 2008) (K A Snyder, Ferraris, Martys, & Garboczi, 2000). Since then, other concrete electrical test methods have been developed that are non-destructive and simpler to perform. These tests, while all based on the same general physics, each have unique features and issues that merit further examination.

2.7.1 Rapid Chloride Permeability Test (RCPT)

The rapid chloride permeability test (RCPT) is a popular test method that is currently performed based on the electrical concept. This test has existed for more than three decades and was standardized as ASTM C1202 in 1991 (whiting, 1980) (Bentz, 2007)

The RCPT provides a rapid indication of concrete resistance to the chloride ion penetration by measuring the total charge driven across a concrete sample by an applied 60-V electrical potential (ASTM C1202, 2012). This test method involves at least 2 days of preparation. The samples need to be cut into 2 in. thick slices and placed in a vacuum desiccator with both ends exposed. The vacuum is maintained for three hours in the desiccator, and then filled with de-aired water and maintained for an additional hour. After that, the samples should be left soaked for 18 ± 2 hours. The 2 in. thick samples are then placed inside a testing cell with one side of the cell filled with 3.0 % sodium chloride (NaCl) and the other side filled with 0.3M sodium hydroxide (NaOH) solutions, as shown in Figure 2-1. The electrical charge passed between the electrodes is integrated with time using readings taken every 30 minutes during the six-hour testing period (ASTM C1202, 2012). Even though this test has been adopted as a standard test, there have been number of criticisms of this technique (Shane et al., 1999)(Riding et al., 2008). First, the current that passes through the sample is dependent on the pore solution conductivity. For example, admixtures such as calcium nitrite corrosion inhibitors are known to increase the pore solution conductivity and charge passed (ASTM C1202, 2012). Second, the high voltage applied can lead to specimen heating, giving misleadingly high results (Shane et al., 1999)(Riding et al., 2008). Third, since it is a destructive test, it cannot be used again due to physical and chemical change. This test has a high variability, and the precision statement in ASTM 1202 indicates that single and multilaboratory measurements will have a coefficient of variation of 12.3% and 18 %, respectively (ASTM C1202, 2012). Thus, the results from two properly conducted tests on the same material in the same lab and different lab could differ by as

much as 42% and 51%, respectively. Typically, three averaged samples are used to reduce the multilaboratory variation to 29% (Joshi & Chan, 2002).

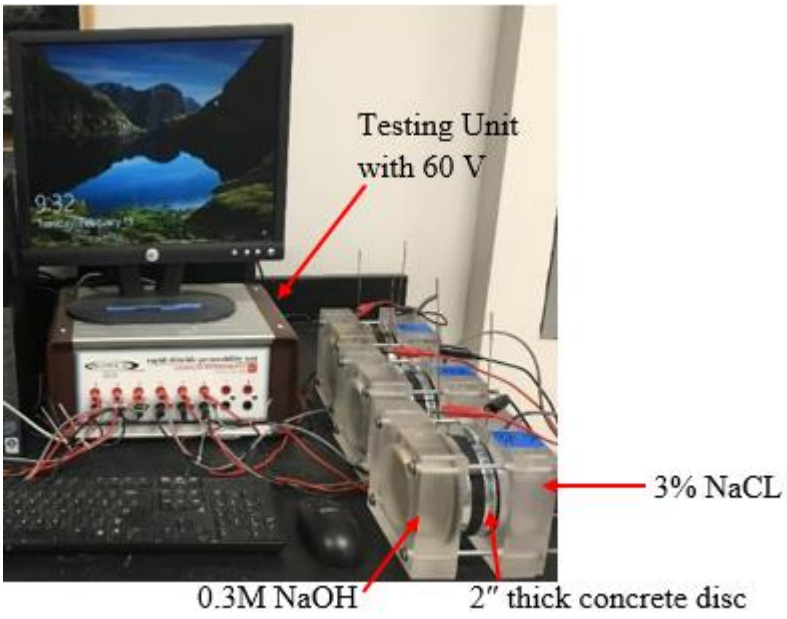

Figure 2-1: RCPT samples during testing (Photo credit: Raid Alrashidi)

2.7.2 Surface Resistivity

The surface resistivity test can be used to evaluate the electrical resistivity of a saturated concrete cylinder to provide an estimation of its permeability. One of the most common techniques for measuring the surface resistivity is a four-probe technique first developed by Frank Wenner in order to determine soil strata. It was later modified for concrete use and is often called a Wenner probe (Wenner, 1916). In this technique, four equally spaced electrode are located on concrete surface to measure the potential difference caused by the applied current (Proceq SA, 2016) as shown in Figure 2-2:

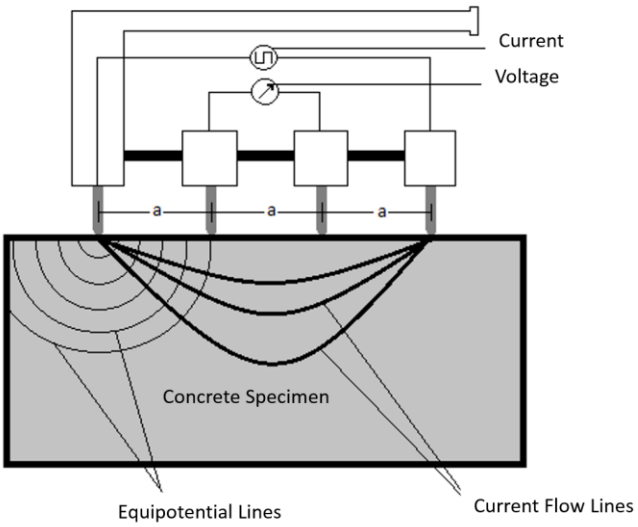

Figure 2-2: Four-point wenner probe

The electrical resistance is affected by a number of factors such as, humidity, pore solution conductivity and temperature. Therefore, care should be taken when measuring the electrical resistivity, which can be calculated using the Equation 2-4:

$$\rho = 2\pi a \,.\left(\frac{V}{I}\right) \tag{2-4}$$

Where is ρ the concrete surface resistivity (Ω-cm), V is the voltage measured between two inner probes (V), I is the applied current by the two exterior probes (A), and a is the probe tip spacing (cm)

Probe spacing must be taken into account as it will affect the obtained results. If the probe spacing is too small, a high degree of scatter can occur in the presence of the aggregate (Shahroodi, 2010). Too large of a probe spacing can lead the electrical current to penetrate more into the concrete layers (R. Polder et al., 2000). To reduce the variance in resistivity measurements, an electrode spacing between 20mm and 70mm is typically used (Sengul & Gjørv, 2009)(Morris, Moreno, & Sagüés, 1996). Probe spacing is recommended to be 1.5 times higher than the maximum aggregate size

(Gowers & Millard, 1999). An electrode spacing of 1.5 inch (38 mm) is considered standard for AASHTO TP 119 (AASHTO, 2015).

A precision statement for concrete surface resistivity was developed for use with LADOT and states that if two tests properly performed by a single operator should not differ from their average by more than 13.28%, and two tests performed by different laboratories should not vary by more than 34.55% (Rupnow & Icenogle, 2011)(R. P. Spragg, Castro, Nantung, Paredes, & Weiss, 2012).

2.7.3 Bulk Resistivity

The bulk resistivity test is a non-destructive test that can be used to measure the electrical resistivity of saturated concrete to provide a rapid indication of its resistance to chloride ion penetration. This test method can use the same equipment (4-pronged Wenner probe) as surface resistivity to measure the resistance of the cylinder with the probe tips attached to conductive plates placed on the end of the cylinder. Saturated sponges or conductive gel are typically used between the conductive plates and the ends of the cylinder, as shown in Figure 2-3.

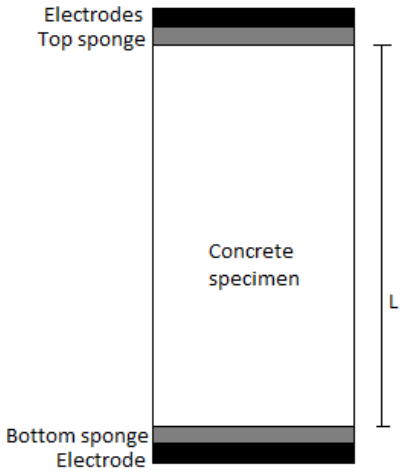

Figure 2-3: Bulk resistivity set-up

The resistance of the saturated sponges should be measured prior to testing and subtracted from the total resistance of the system by using the Equation 2-5:

$$R_{cylinder} = R_{measured} - R_{top\ sopnge} - R_{bottom\ sponge} \quad (2\text{-}5)$$

Where, $R_{cylinder}$ the calculated bulk resistance (Ω), and $R_{measured}$ is the measured resistance of the probe (Ω). The bulk resistivity is then calculated using the Equation 2-6:

$$\rho = R_{cylinder} \times K \quad (2\text{-}6)$$

Where ρ is the resistivity of the concrete (kΩ.cm), and K is the geometry factor which is the ration of the cross-sectional area A (cm^2) to the length of the specimen L (cm) as shown in Equation 2-7.

$$K = \frac{A}{L} \quad (2\text{-}7)$$

A precision statement developed by LADOT indicates that the automated resistivity measurements within-laboratory have a coefficient of variation of around of 4.36 %, and the multi-laboratory coefficient of variation of 13.22 % (R. P. Spragg et al., 2012).

2.8 Factors Affecting the Resistivity Measurements

The electrical resistivity of concrete can be affected by several factors. These factors can be divided into two groups: the first group is intrinsic factors that is related to concrete characteristics such as: w/c ratio, aggregate size and type, hydration, and pore structure. The second group is extrinsic factors related to testing conditions such as specimen geometry, temperature, moisture content, and the electrode signal frequency.

2.8.1 Intrinsic Factors

2.8.1.1 Water-Cementitious Materials Ratio (w/cm)

Water to cementitious materials ratio (w/cm) plays an important role in the permeability of concrete and its properties. W/cm represents the gel porosity and evaporable water in concrete. An increase in the w/cm results in a high percentage of porosity, higher pore fraction within the cement and lower electrical resistivity values, indicating a more permeable concrete (Rupnow & Icenogle, 2012) (Van Noort, Hunger, & Spiesz, 2016).

2.8.1.2 Aggregate Size and Type

Most aggregates have a higher electrical resistivity than hardened cement paste because they have less porosity. Most electrical conductance occurs in the paste portion of the concrete (Azarsa & Gupta, 2017). By this same logic, higher aggregate content results in higher electrical resistivity (Morris et al., 1996). For the same aggregate content, mixtures containing large aggregate (16-32mm) had higher resistivity compared with small particle size (0-4 mm), and three times higher than that of the cement paste (Sengul, 2014). Although most of the electrical conductance occurs in the paste, aggregate types can affect the properties of concrete. For the same aggregate volume percentage, electrical resistivity were higher for the crushed limestone than the rounded siliceous gravel, and the surface texture might be a possible cause for that, in which the gravel had smooth surface resulting in poor bonding (Sengul, 2014). The effect of aggregate type, content, and size should not be ignored when doing the resistivity tests. Also, when comparing the resistivity values of different concretes, they should be taken into account.

2.8.1.3 Sample Curing Conditions

The curing regimes and concrete composition influence the resistivity of concrete evolution with time (Presuel-Moreno, Wu, & Liu, 2013)(R. Spragg, Villani, et al., 2013). The type of curing has an impact on the electrical pore solution resistivity measurements. It can cause changes in readings by 80% (Bu & Weiss, 2014). The degree of saturation and the degree of hydration of the specimen can develop differences in resistivity measurements. The degree of hydration and saturation, the pore structure, and solution through leaching can be influenced by the sample storage and curing condition (Weiss, Snyder, Bullard, & Bentz, 2012). Storing the samples underwater or saturated lime water affect the resistivity measurements through leaching of alkalis and can increase the degree of hydration. To correct for this difference in readings, the samples cured in lime water, the average resistivity readings should be multiplied by 1.1 (AASHTO, 2015). Increased saturation provides for more pores that can conduct electricity and increases pore solution conductivity, which effects the measured resistivity.

When compared to sealed curing, storing in a saturated lime water showed a decrease in the conductivity of the pore solution by an order of magnitude due to leaching of alkalis from the pore solution to the storage solution and less connected pore water (Bu & Weiss, 2014).

Simulations of a mortar with a w/cm of 0.42 were performed with three curing conditions: a) specimens sealed on both curing and testing, b) specimens sealed during curing and saturated during testing, c) specimens saturated on both curing and testing (Weiss et al., 2012)(Weiss et al., 2012)(Bullard et al. 2008). The results showed that the specimens that were sealed for both curing and testing had the highest resistivity while

specimens sealed during the curing and saturated during testing had the lowest resistivity because of the lower degree of hydration.

2.8.1.4 Pore Solution Composition

Pore solution analysis and composition of concrete are highly significant for understanding the ongoing hydration reactions and interpreting electrical resistivity measurements. The pore solution of cementitious materials is composed of potassium (K^+), sodium (Na^+), calcium (Ca^{2+}), sulfate $(SO_4)^{2-}$, and hydroxides (OH^-) ions. Supplementary of cementitious materials (SCMs) can alter the concrete pore solution composition. in which they can consume the hydroxyl ions (OH-), which leads to an increase the electrical resistivity compared to the referenced concrete sample (C. Shi, 2004).

Pore solution expression was first used in 1970 by Longuet, burglen, and modified by Barneyback (Barneyback et al., 1981). This technique is performed by placing the cement paste samples into a highly pressurized die system and applying a mechanical load of up to 550 MPa. The specimen is then squeezed to remove the pore solution. The pore solution is collected in a small syringe for measuring its composition or resistivity (Barneyback et al., 1981). It is recommended that the electrical resistivity of the pore solution be measured immediately to avoid any potential for carbonation, evaporation (Tsui-Chang, M, 2017) or other change in the chemical composition.

Another experimental method for obtaining the pore solution conductivity is a pore solution electrical conductivity sensing system. The system consists of two sensors that are made from a porous material connected to electrodes on both ends as shown in Figure 2-4. The sensor is calibrated by using different salt solution such as KOH, NaOH, and NaCL to account for the moisture and temperature effect , and prior to placement,

the sensor should be vacuum saturated, dried to 1% relative humidity and infiltrated by a 0.4 of KOH solution (Rajabipour et al., 2007). The sensors can then be placed inside a concrete specimen during casting. The fluid conductivity inside the sensor should come to equilibrium with that of the concrete pore solution. The conductivity of the sensors inside the concrete specimens can be used to determine the pore solution conductivity (Rajabipour et al., 2007)

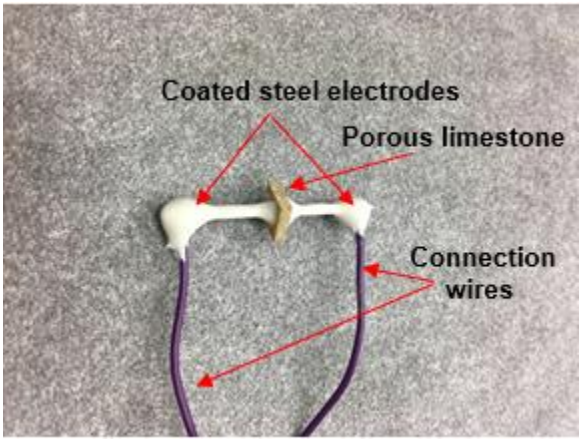

Figure 2-4: The pore solution conductivity sensor (Photo credit: Raid Alrashidi)

The pore solution can be estimated by using a pore solution conductivity calculator, such as http://concrete.nist.gov/poresolncalc.html , in which the procedure was originally described by Taylor (1987). This method estimates the pore solution based on the mixture proportions, degree of hydration, and the alkali content of the cementations materials (Bentz, 2007). Even though this method allows for an estimate of the pore solution conductivity when it is impractical to measure, it has some shortcomings. This method doesn't account for the reaction of sulfate that occur early in the first 24 hours. Some SCMs such as silica fume can bind alkalis. The calculator estimates that 75% of the total amount of alkali from the cement (Na+, and K+), fly ash, slag, and silica fume are present after the first 24 hours in the pore solution (De La Varga et al., 2014). This

is a great simplification, since silica fume can release bound alkalis into the pore solution at later ages (M. Thomas, Fournier, & Folliard, 2006). Also, it doesn't account for all the chemical composition of all the supplementary cementitious materials such as metakaolin or emerging SCMs.

2.8.2 Extrinsic Factors

2.8.2.1 Specimen Geometry

Many sample geometries have been used to measure the resistivity of concrete. The resistivity of concrete (ρ) can be determined by measuring the electrical resistance (R) and applying appropriate geometry factor (K) converts the resistance to a resistivity as shown in Equation 2-8:

$$\rho = R \times K \tag{2-8}$$

The correction factor to measure the resistivity can be calculated using the Equation 2-9:

$$K_1 = 1.10 - \frac{0.730}{d/a} + \frac{7.34}{\left(d/a\right)2} \tag{2-9}$$

Where K_1 is the geometry factor, and d is the specimen diameter (cm). This geometry correction is only valid for specimens with $d/a \leq 4$ and $L/a \geq 5$.

Many commercial surface resistivity meters such as the Proceq Resipod automatically applies the correction factor K_2 given in the Equation 2-10:

$$K_2 = 2\pi a \tag{2-10}$$

In this case, the correction factor for the surface resistivity test should be calculated using the following Equation 2-11:

$$K_{surface} = \frac{1}{K_1} \quad (2\text{-}11)$$

However, if the resistivity meter displays just the measured resistance, the correction factor should be calculated using the Equation 2-12:

$$K_{surface} = \frac{K_2}{K_1} \quad (2\text{-}12)$$

For bulk resistivity tests (two-electrode method) in which the electrical current passes through the whole cylinder to measure the resistance, the resistivity can be calculated using Equation 2-7.

2.8.2.2 Specimen temperature

The temperature variation of the sample has been reported to greatly influence the measured resistivity (Michelle, Adam, Xiaorong, & Douglas, 2017)(McCarter, Starrs, & Chrisp, 2000). The temperature can affect the flow of the electrical current through the ions dissolved in the pore solution by changing the ion mobility as well as the ion concentration in concrete (Villagrán Zaccardi, García, Huélamo, & Di Maio, 2009)(R. B. Polder, 2001). Higher temperature increases the movement of ions into the pore solution of concrete and decreases the electrical resistivity measurements (R. Spragg, Villani, et al., 2013). Since the temperature plays an important role in the variation of the concrete resistivity measurements, it has been proposed to account for temperature variations (Liu & Presuel-Moreno, 2014)(Villagrán Zaccardi et al., 2009)(McCarter, Chrisp, Starrs, Basheer, & Blewett, 2005) by using the Arrhenius law as shown in Equation 2-13:

$$\frac{\rho_T}{\rho_0} = exp\left[\frac{E_{a,\rho}}{R}\left(\frac{1}{T} - \frac{1}{T_0}\right) \right] \quad (2\text{-}13)$$

Where ρ_T is the resistivity of concrete (Ω.m) T at temp (℃), ρ_0 is the concrete resistivity (Ω.m) at reference temp T_0 (typically 23℃), R is the universal gas constant, (8.314 J/mol.k) and $E_{\alpha,\rho}$ is the activation energy of conduction (KJ/mol) which represents the effect of the testing temperature. $E_{\alpha,\rho}$ is different than the activation energy of hydration that describes the effect of temperature on the hydration process (Coyle, Spragg, Suraneni, Amirkhanian, & Weiss, 2018)

If the temperature ranges between 22.7 to 24.4 ℃, the effect of the temperature is not significant as the temperature factor varies from 0.97 to 1.02 (Paredes et al., 2012)(Kamtornkiat Musiket; Mitchell Rosendahl; and Yunping Xi, 2016)(R. P. Spragg et al., 2012). Nevertheless, it is mentioned that in the AASHTO standards for a standard curing condition the concrete samples should always be tested at standard temperature 20 to 25 ℃ (68 to 77 ℉) (AASHTO, 2015). However, large temperature variations are typically noticed in practice, therefore, the correction should be made when required.

2.8.2.3 Signal Frequency

Due to high polarization effects on the electrodes when using direct current (DC) alternating current (AC) is used to measure the electrical resistivity of concrete (R. Polder et al., 2000)(Gowers & Millard, 1999). For the electrical resistivity measurements, the two signal AC current shapes that frequently used are sine-wave or square-wave (Azarsa & Gupta, 2017). The impedance spectrum in general comprises of two arcs in the high and low-frequency ranges. The characteristics of the impedance spectrum at high and low frequencies are mainly attributed to the microstructure of concrete and the conditions at the electrode-concrete interface (Layssi, H, 2009). A frequency range of 0.5 to 10 kHz is usually used for the resistivity measurements in the

uniaxial method; however, since there are many other factors that can affect the electrical resistivity of concrete such as environment conditions, there is no uniform optimum frequency across mixtures (Layssi, H, 2009). Resistivity values are generally overestimated at frequencies below 500 Hz because of the electrode–concrete interface. Compared to the 1 kHz signal frequency, using a 40 Hz signal had a 9% higher measured resistivity. (Layssi, H, 2009).

2.9 Summary

This chapter has presented a literature review about the electrical properties of concrete as they become popular method and a quality control indicator. RCP test has become an old method and since it has shortcomings, the surface and bulk resistivity have been used dramatically as a non-destructive and for their simplicity. However, when measuring the electrical resistivity, several factors can affect the obtained results. These factors can be summarized and divided in to two group; the first group is the intrinsic factors include the following:

W/cm: an increase in the w/cm results in a high percentage of porosity, higher pore fraction within the cement, thus it leads to lower electrical resistivity values (Rupnow & Icenogle, 2012) (Van Noort et al., 2016)

- **Aggregate size and type:** electrical resistivity is higher for mixtures having large aggregate.
- **Curing condition**: the curing regimes can highly influence the resistivity measurements due to leaching. Therefore, sealed curing still the best option since it eliminates the leaching effect.
- **Pore structure:** pore solution analysis is significant for understanding the ongoing hydration reactions and interpreting electrical resistivity measurements. Pore solution expression, sensors to put inside the fresh concrete, and NIST calculator are the way to obtain and estimate the pore solution conductivity.

The other group is the extrinsic factors include the following:

- **Sample geometry:** many commercial resistivity meters display the resistance- not the resistivity- and overestimate the obtained measurements, therefore, applying the geometry factor must be taken into account to convert the resistance to resistivity.

- **Sample temperature:** as the temperature increases, they change the ion mobility in the pore solution leading to a decrease in the resistivity measurements (R. Spragg, Villani, et al., 2013). Therefore to account for that, Arrhenius law can be used as shown in Equation 2-13.

- **Electrode signal frequency:** resistivity values are generally overestimated at frequencies below 500 Hz because of the electrode–concrete interface.

In general, incorporation of SCMs can enhance concrete fresh properties such as workability, setting time, and heat of hydration, and its mechanical properties such as strength. Due to their pozzolanic reaction and the filling effect, they alter the pore solution, thus the permeability is lowered.

CHAPTER 3
MATERIALS

Four different types of cements were used in this project, an ASTM C150 Type I/II, Type IV, Type IL11, and a Type I cement with a high alkali content (HA) (ASTM, 2017). These cements with different compositions were selected to address the effect of chemical composition on measured electrical properties of concrete. ASTM C150 (ASTM, 2007) Type I/II cement is the most commonly used cement in Florida. ASTM C150 (ASTM, 2007) Type V cements with a C_3A content of 2.2% was used. The Type IL(11) used has 11% limestone fillers interground with the cement, in which the limestone fines help improve the cement's plastic properties, strength, and durability (Vuk, Tinta, Gabrovšek, & Kaučič, 2001). The high alkali (HA) cement with a Na_2O_{eq} content of 0.86% was procured for use. The cement chemical composition is presented in Table 3-1

Four different types of supplementary cementitious materials (SCMs) were used in this study, fly ash, slag cement, silica fume, and metakaolin to assess their effects on the concrete electrical properties. All cements and fly ash chemical compositions were measured using a Rigaku Supermini x-ray fluorescence (XRF) machine. The slag cement, silica fume, and metakaolin compositions were analyzed by CTL Group. The chemical composition of SCMs used in this study are presented in Table 3-1

Table 3-1: Cement and Supplementary Cementitious Material Composition as Measured by XRF

Material	SiO_2	TiO_2	Al_2O_3	Fe_2O_3	MnO	MgO	CaO	Na_2O	K_2O	P_2O_5	LOI
	wt%	wt%	wt%	wt%	wt%	wt%	wt%	wt%	wt%	wt%	wt%
Cement IL(11)	19.93	0.39	4.47	3.63	0.02	0.86	64.03	0.07	0.33	0.10	5.21
Cement type V	20.83	0.21	4.12	3.88	0.16	0.87	66.24	0.02	0.62	0.11	2.86
Cement type I/II	21.00	0.23	5.06	3.28	0.08	0.68	66.74	0.10	0.24	0.15	3.02
High alkali cement	20.56	0.21	4.55	3.78	0.09	3.06	63.65	0.29	0.87	0.12	2.68
Class F Fly Ash	48.59	1.00	19.49	19.68	0.04	0.84	5.08	0.83	2.09	0.12	1.88
Slag	34.1	0.58	14.04	0.59	0.25	5.45	41.27	0.23	0.24	0.01	0.47
Silica fume	87.67	<0.01	0.34	0.89	0.09	6.71	0.63	0.75	0.99	0.10	3.12
Metakaolin	52.53	1.8	42.96	1.49	<0.01	0.18	<0.01	0.05	0.14	0.15	1.46

3.1 Aggregates

The aggregate used in this study were selected to be representative of FDOT mixtures and are compatible with the test requirements. The No. 57 coarse aggregate used was a Miami Oolite limestone. The specific gravity and absorption were measured according to ASTM C127 (ASTM, 2015a) as shown in Table 3-2. The fine aggregate used was a natural silica sand. Its specific gravity and absorption were measured according to ASTM C128 (ASTM, 2015b) as shown in Table 3-3.

Table 3-2: Coarse Aggregate Specific Gravity and Absorption

Bulk specific gravity dry	2.29
Bulk specific gravity SSD	2.40
Apparent specific gravity	2.56
Absorption	4.66 %

Table 3-3: Fine Aggregate Specific Gravity and Absorption

Relative Density (Specific Gravity) (Oven Dry)	2.599
Relative Density (Specific Gravity) (Saturated Surface Dry)	2.605
Apparent Relative Density (Specific Gravity)	2.614
Absorption	0.22 %

3.2 Mixtures

Thirty-eight different concrete mixtures were made for this study, including ternary and binary cementitious mixtures with water-cementitious materials ratio (w/cm) of 0.35, and 0.44. Twenty-two concrete mixtures were made with an ASTM C618 (ASTM, 2010a) Class F fly ash (FA) at a 10 or 20% equivalent weight replacement of portland cement. Ten concrete mixtures were made with an ASTM C989 (ASTM, 2013a) grade 120 slag cement (G) at 30, 45, 55 or 60 % equivalent weight replacement of portland cement. Nine concrete mixtures were made with an ASTM C1240 (ASTM,

2012)-compliant silica fume (S) at 4, 6, or 8 % equivalent weight replacement of portland cement. Nine concrete mixtures were made with an ASTM C618 (ASTM, 2010a) Metakaolin at 6, 8, or 10% equivalent weight replacement of Portland cement. Table 3-4 shows the mixture proportions used in this research.

Table 3-4: Mix proportions for concrete

Mix No	Mix ID	W/C	weight per yd^3 (LB)							Admixtures (ml)		
			Cement	Fine aggregate	Coarse aggregate	FA	SF	S	MK	AEA	WRDA 60	ADVA 120
1	C-100	0.35	700	1184	1680	-	-	-	-	12.0	180.7	132.5
2	C-100h	0.44	700	1190	1552	-	-	-	-	6.0	6.0	0.0
3	C-F10	0.35	630	1167	1680	70	-	-	-	12.0	180.7	114.5
4	C-F20	0.35	560	1150	1680	140	-	-	-	12.0	180.7	114.5
5	C-F10h	0.44	630	1145	1552	70	-	-	-	6.0	6.0	0.0
6	C-F20h	0.44	560	1130	1552	140	-	-	-	6.0	6.0	0.0
7	C-G60	0.35	280	1175	1680	-	420		-	12.0	180.7	212.1
8	C-S8	0.35	644	1188	1680	-	-	56	-	12.0	180.7	132.5
9	C-M10	0.35	630	1193	1680	-	-	-	70	12.0	180.7	132.5
10	C-F10G30	0.35	420	1172	1680	70	210	-	-	12.0	180.7	132.5
11	C-F10G45	0.35	315	1164	1680	70	315	-	-	12.0	180.7	132.5
12	C-F10G60	0.35	210	1156	1680	70	420	-	-	12.0	180.7	183.7
13	C-F10G60h	0.44	210	1140	1552	70	420	-	-	6.0	6.0	50.6
14	C-F20S4	0.35	532	1161	1680	140	-	28	-	12.0	180.7	132.5
15	C-F20S6	0.35	518	1157	1680	140	-	42	-	12.0	180.7	210.8
16	C-F20S8	0.35	504	1152	1680	140	-	56	-	12.0	210.8	210.8
17	C-F20S8h	0.44	504	989	1680	140	-	56	-	12.0	180.7	0.0
18	C-F20M6	0.35	518	1161	1680	140	-	-	42	12.0	180.7	210.8
19	C-F20M8	0.35	504	1159	1680	140	-	-	56	8.4	210.8	241.0
20	C-F20M10	0.35	490	1155	1680	140	-	-	70	6.0	210.8	277.1
21	C-F20M10h	0.44	490	995	1680	140	-	-	70	12.0	90.4	99.4
22	C-G55S8	0.35	259	1160	1680	-	56	385	-	12.0	180.7	198.8
23	C-G55M10	0.35	245	1164	1680	-	-	385	70	12.0	180.7	210.8
24	CV-100	0.35	700	1185	1680	-	-	-	-	12.0	180.7	132.5
25	CV-100h	0.44	700	1190	1552	-	-	-	-	6.0	6.0	0.0
26	CV-F10G60	0.35	210	1156	1680	70	420	-	-	12.0	180.7	132.5
27	CV-F20S8	0.35	504	1153	1680	140	-	56	-	12.0	180.7	132.5
28	CV-M10	0.35	630	1193	1680	-	-	-	70	12.0	180.7	132.5

Table 3-4. Continued.

Mix No	Mix ID	W/C	weight per yd^3 (LB)							Admixtures (ml)		
			Cement	Fine aggregate	Coarse aggregate	FA	SF	S	MK	AEA	WRDA 60	ADVA 120
29	CL-100	0.35	700	1184	1680	-	-	-	-	12.0	180.7	132.5
30	CL-100h	0.44	700	1165	1552	-	-	-	-	6.0	6.0	0.0
31	CL-F10G60	0.35	210	1156	1680	70	420	-	-	12.0	180.7	132.5
32	CL-F20S8	0.35	504	1152	1680	140	-	56	-	12.0	180.7	132.5
33	CL-M10	0.35	630	1192	1680	-	-	-	70	12.0	180.7	241.0
34	CHA-100	0.35	700	1184	1680	-	-	-	-	12.0	180.7	132.5
35	CHA-100h	0.44	700	1165	1552	-	-	-	-	6.0	6.0	0.0
36	CHA-F10G60	0.35	210	1156	1680	70	420	-	-	12.0	180.7	132.5
37	CHA-F20S8	0.35	504	1152	1680	140	-	56		12.0	180.7	132.5
38	CHA-M10	0.35	630	1192	1680	-	-	-	70	12.0	180.7	241.0

CHAPTER 4
METHODOLOGY

4.1 Concrete Methodology

Cylinders used for measuring concrete electrical properties were made according to ASTM C192 “Standard Practice for Making and Curing Concrete Test Specimens in the Laboratory”(ASTM, 2016). All concrete batches were made in the concrete mixing facilities at the University of Florida (UF).

4.2 Concrete Mixing

Three days prior to mixing, the coarse aggregate was soaked in a water tub and the fine aggregate was oven dried at 230°F (110°C). One day prior to mixing, all the materials including aggregates and cementitious materials were weighed and sealed using 5-gallon buckets. On the day of mixing, the mixer was rinsed with water to clean it and then buttered with fine aggregates, cement and water to compensate for mortar loss when the fresh concrete was discharged from the mixer. After that, the coarse and fine aggregate were added to the mixer and mixed for 30 seconds. While the mixer was running, the cementitious materials and more than half of the mixing water were added. Chemical admixtures and the remaining water were added gradually over about 1 minute. The total mixing time for adding all the materials was 3 minutes, followed by a 3-minute rest, and by mixing for 2 additional minutes. After the mixing was done, the fresh concrete properties were measured.

4.3 Fresh Concrete Properties

Standard concrete fresh quality control tests were performed. Concrete slump was measured according to ASTM C143 “Standard Test Method for Slump of Hydraulic-Cement Concrete” (ASTM, 2015c) as shown in Figure 4-1. The slump was maintained

between 2 and 8 in. (51 and 203 mm). Measured concrete fresh properties are shown in Table 4-1.

Figure 4-1: Determination of slump (Photo credit: Raid Alrashidi)

The unit weight test is used to measure the density of fresh concrete for quality control purposes and can help pick up problems with incorrect ingredients or air content. This test was performed according to ASTM C138 “Standard Test Method for Density (Unit Weight), Yield, and Air Content (Gravimetric) of Concrete” (ASTM, 2013b) as shown in Figure 4-2.

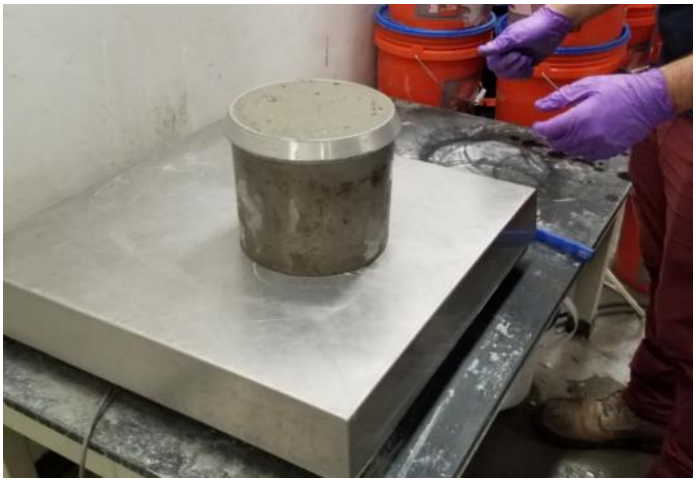

Figure 4-2: Determination of unit weight (Photo credit: Raid Alrashidi)

Table 4-1: Measured concrete fresh properties

Mix No	Mix ID	W/C	Slump, in (mm)	Air (%)	Unit weight, lb/ft3 (kg/m3)	Mix Temp, °F (°C)
1	C-100	0.35	6 (152)	3.00%	144 (2310)	74.3 (23.5)
2	C-100h	0.44	7 (165)	2.00%	142 (2280)	74.5 (23.6)
3	C-F10	0.35	4 (102)	3.00%	144 (2303)	74.5 (23.6)
4	C-F20	0.35	6 (140)	4.00%	141 (2259)	75.2 (24)
5	C-F10h	0.44	8 (191)	3.00%	142 (2272)	72.5 (22.5)
6	C-F20h	0.44	8 (203)	3.50%	142 (2269)	72.7 (22.6)
7	C-G60	0.35	5 (127)	2.00%	146 (2331)	72.1 (22.3)
8	C-S8	0.35	2 (51)	3.80%	142 (2277)	72.3 (22.4)
9	C-M10	0.35	3 (64)	2.80%	144 (2302)	72.7 (22.6)
10	C-F10G30	0.35	5 (127)	4.50%	141 (2266)	73.4 (23)
11	C-F10G45	0.35	6 (140)	3.10%	142 (2271)	72 (22.2)
12	C-F10G60	0.35	8 (203)	2.50%	142 (2276)	71.8 (22.1)
13	C-F10G60h	0.44	6 (152)	2.80%	140 (2249)	72.7 (22.6)
14	C-F20S4	0.35	2 (51)	3.00%	143 (2284)	74.8 (23.8)
15	C-F20S6	0.35	3 (64)	3.40%	142 (2282)	75.4 (24.1)
16	C-F20S8	0.35	6 (152)	5.00%	141 (2262)	74.1 (23.4)
17	C-F20S8h	0.44	6 (152)	1.60%	140 (2244)	72.1 (22.3)
18	C-F20M6	0.35	4 (102)	3.40%	141 (2252)	73.8 (23.2)
19	C-F20M8	0.35	2 (51)	4.00%	144 (2305)	73.8 (23.2)
20	C-F20M10	0.35	2 (51)	2.50%	145 (2316)	73.6 (23.1)
21	C-F20M10h	0.44	6 (152)	2.00%	141 (2261)	73.9 (23.3)
22	C-G55S8	0.35	3 (64)	3.50%	140 (2240)	72.5 (22.5)
23	C-G55M10	0.35	2 (51)	2.50%	140 (2240)	72.7 (22.6)
24	CV-100	0.35	3 (64)	2.75%	144 (2309)	74.7 (23.7)
25	CV-100h	0.44	6 (152)	1.50%	140 (2249)	75.4 (24.1)
26	CV-F10G60	0.35	7 (178)	3.00%	142 (2278)	71.8 (22.1)
27	CV-F20S8	0.35	4 (89)	4.50%	140 (2240)	73 (22.8)
28	CV-M10	0.35	3 (70)	3.10%	142 (2267)	72.7 (22.6)
29	CL-100	0.35	4 (108)	3.50%	141 (2258)	76.5 (24.7)
30	CL-100h	0.44	5 (114)	4.00%	140 (2239)	76.8 (24.9)
31	CL-F10G60	0.35	5 (127)	3.20%	142 (2277)	71.6 (22)
32	CL-F20S8	0.35	3 (64)	4.00%	139 (2228)	75.6 (24.2)
33	CL-M10	0.35	2 (38)	2.70%	144 (2307)	75.2 (24)
34	CHA-100	0.35	3 (83)	3.00%	143 (2284)	75 (23.9)
35	CHA-100h	0.44	7 (184)	2.80%	142 (2269)	75.6 (24.2)
36	CHA-F10G60	0.35	5 (114)	3.20%	141 (2255)	71.8 (22.1)
37	CHA-F20S8	0.35	3 (64)	4.00%	140 (2239)	74.8 (23.8)
38	CHA-M10	0.35	2 (51)	2.50%	140 (2239)	74.7 (23.7)

The concrete air content was measured using ASTM C231 “Standard Test Method for Air Content of Freshly Mixed Concrete by the Pressure Method” (ASTM, 2010b) as shown in Figure 4-3.

Figure 4-3: Determination of air content (Photo credit: Raid Alrashidi)

The concrete fresh temperature was measured according to ASTM C1064 “Standard Test Method for Temperature of Freshly Mixed Hydraulic-Cement Concrete” (ASTM, 2004) as shown in Figure 4-4. Since the concrete mixtures were all mixed in a temperature controlled laboratory, the concrete temperature measured was between 71.6 and 75.6°F (22 and 24.2°C).

Figure 4-4: Concrete Temperature Measurement (Photo credit: Raid Alrashidi)

4.4 Concrete Specimen Preparation

After measuring the fresh concrete properties, 4 × 8 in. (100 × 200 mm) concrete cylinders were made according to ASTM C192 procedure (ASTM, 2016). The concrete was placed into the cylinder molds in two equal layers as shown in Figure 4-5. The concrete samples were consolidated using vibration from a vibrating table. After the concrete was placed in the cylinder molds, they were finished and capped to prevent moisture loss during the first 24 hours after mixing.

Figure 4-5: Cylinders after filled with the first layer of concrete (Photo credit: Raid Alrashidi)

4.5 Concrete Curing

The concrete specimens were removed from molds 24 ± 8 hours after mixing. All but three samples from each mixture were stored in a moist curing room until they were ready for testing or further sample preparation. The moist curing room was kept between 70 and 77°F (21 and 25°C) and above 95% relative humidity.

4.6 Simulated Pore Solution (SPS) Curing Method

After demolding, three concrete specimens were chosen to put in a sealed container. The NIST calculator developed by Bentz and available at (http://concrete.nist.gov/poresolncalc.html) was used to estimate the electrical conductivity (S/m) (inverse of the resistivity) of the concrete pore solution for each mixture. The material oxide composition measured for each material using x-ray fluorescence and given in Table 3-1 was used in the calculations. The system degree of hydration was estimated to be 70% in the calculations. Since use of metakaolin was not an option in the calculator, and the content of K_2O and Na_2O for metakaolin was close to that of slag, the slag option was used instead.

Therefore, after getting all the information from the calculator, the specimens were placed into six liters of a NaOH and KaOH solution in a 5-gallon bucket and sealed, as shown in Figure 4-6. A minimum of three grams per liter of $Ca(OH)_2$ was added to prevent calcium hydroxide leaching of the species. After that, the container was stored in a moist curing room to maintain the temperature until they are ready for testing. On the day of testing, the surface and bulk resistivity measurements were taken, as well as the pore solution conductivity was taken by using an Oakton PC700 Meter as shown in Figure 4-7.

Figure 4-6: The specimens were placed in a sealed container (Photo credit: Raid Alrashidi)

Figure 4-7: Oakton PC700 Meter (Photo credit: Raid Alrashidi)

4.7 Electrical Tests

4.7.1 Surface Resistivity

Concrete surface resistivity was measured in this project according to AASHTO T358 (AASHTO, 2011) to provide a rapid indication of the concrete's potential durability. A Proceq Resipod surface resistivity meter was used in this project, as shown in Figure

4-8. The specimen holder used to mark specimen points for measurement is shown in Figure 4-9.

Figure 4-8: Surface resistivity meter used in this study (Photo credit: Raid Alrashidi)

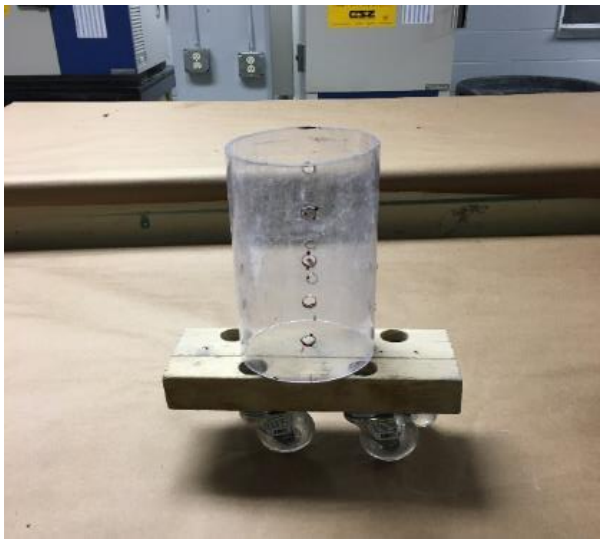

Figure 4-9: Specimen holder used in this study (Photo credit: Raid Alrashidi)

Immediately after demolding the concrete cylinders, three specimens were chosen to be used for surface resistivity testing. Four marks were made at 0, 90, 180, and 270-degree points around the circumference of the samples before the samples were placed in the fog room. On the day of testing, the samples were removed from the fog room, and kept saturated during the testing time. The cylinder was then laid on the

top of the holder and four measurements were taken around the circumference of the cylinder at 90-degree increments with the resistivity meter, as shown in Figure 4-10. This process was repeated to get the average for the eight total readings. After all the readings were taken for the three specimens, they were kept saturated to perform the bulk resistivity test.

Figure 4-10: Surface resistivity measurement (Photo credit: Hossein Mosavi)

4.7.2 Bulk Resistivity

This concrete bulk resistivity was measured according to AASHTO TP 119 (AASHTO, 2015) to provide a rapid indication of concrete mixture potential durability. The difference between bulk and surface resistivity tests is with bulk resistivity, the electrical current passes along the height (bulk) of the cylinder, while with the surface resistivity, the electrical current passes across the outer probes of the Wenner probe.

Prior to testing, the concrete specimen end faces were ground with a grinding machine per (ASTM, 2013c), as shown in Figure 4-11. To measure the concrete bulk

resistivity, the plates were attached to the probe tips of the surface resistivity meter. Every two probe tips were connected to one plate. The sponges were saturated, and their resistance was recorded to provide a correction for their resistance, as described in Equation 7. After recording the sponges' resistivity, the bottom sponge was placed on the bottom plate, and the top sponge was placed on the top plate. After that, the concrete specimen was placed between the plates and the reading was taken as shown in Figure 4-12. After recording the concrete specimen's resistivity, the temperature of the cylinder was taken using an infrared thermometer. These steps were performed for the other two specimens and the specimens were then placed back into the fog room until the next testing age.

Figure 4-11: Grinding samples for bulk resistivity measurement (Photo credit: Raid Alrashidi)

Figure 4-12: Bulk resistivity test (Photo credit: Hossein Mosavi)

CHAPTER 5
RESULTS AND DISCUSSION

5.1 Introduction

Thirty-eight different concrete mixtures were made for this project, including four types of cements and four types of SCMs materials. All samples made to measure concrete electrical resistivity properties were cured using one of two methods, moist room curing or simulated pore solution (SPS). In this study, measurements were taken at 28 days, 56 days, and 91 days to see the effect of w/c ratio, incorporation of SCMs, and curing methods on the electrical properties of concrete.

5.2 Pore Solution Conductivity

Based on the mix proportion and the chemical composition, the NIST pore solution calculator was used to estimate the pore solution composition and electrical conductivity for each mixture made. In addition to measuring the solution conductivity when made, it was measured at 28, 56, and 91 days in the bucket used for curing using an Oakton PC700 Meter as shown Figure 4-7. Immediately before measuring the conductivity, the solution was agitated slightly to have a homogenous solution. The conductivity readings for all mixes are presented in Table 5-1. The readings indicate that for most of the mixes, the conductivity readings are less than the estimated readings by NIST calculator, and it was noticed the readings were decreased with time due to the small variability in temperature and leaching.

Table 5-1: Pore solution conductivity readings

Mix #	Mix ID	SPS readings for pore solution Conductivity S/m NIST pore solution S/m	28 days	56 days	91 days
1	C-100	69.6	69.70	69.40	69.50
2	C-100h	48.7	53.00	52.80	53.30
3	C-F10	115.8	73.70*	71.70*	71.00*
4	C-F20	158.8	72.50*	70.90*	71.00*
5	C-F10h	81.8	77.80	77.60	77.00
6	C-F20h	112.9	111.20	109.10	102.50
7	C-G60	29.9	84.70*	85.70*	84.90*
8	C-S8	73.7	71.90	70.80	70.40
9	C-M10	63.2	61.70	60.10	58.80
10	C-F10G30	98.2	97.50	97.10	96.30
11	C-F10G45	89.2	87.20	87.10	87.30
12	C-F10G60	89.9	88.40	88.00	87.30
13	C-F10G60h	56.2	55.20	54.10	53.60
14	C-F20S4	149.9	140.7	139.4	138.6
15	C-F20S6	145.6	138	138.4	137.6
16	C-F20S8	141.5	137.8	136.9	135.2
17	C-F20S8h	100.4	91.20	86.30	82.60
18	C-F20M6	155.5	118.7	116.7	111.7
19	C-F20M8	154.4	145.8	145.5	142.7
20	C-F20M10	153.3	142.3	142.1	141.9
21	C-F20M10h	108.9	103.00	92.80	91.30
22	C-G55S8	47.1	44.80	44.10	44.30
23	C-G55M10	26.4	27.10	26.90	27.20
24	CV-100	113.9	111.10	111.20	109.20
25	CV-100h	80.4	78.80	79.00	78.70
26	CV-F10G60	93.4	92.00	91.30	88.50
27	CV-F20S8	163.3	158.50	155.50	151.00
28	CV-M10	103.7	100.10	96.00	92.00
29	CL-100	77.4	78.50	79.20	79.10
30	CL-100h	54.3	53.60	53.80	53.50
31	CL-F10G60	82.3	80.90	81.50	80.50
32	CL-F20S8	145.2	139.00	133.90	136.20
33	CL-M10	70.3	68.80	66.30	68.40
34	CHA-100	205.1	201.30	201.00	200.60
35	CHA-100h	146.6	145.90	144.50	144.80
36	CHA-F10G60	122.9	121.20	120.90	119.80
37	CHA-F20S8	210.8	192.30	183.60	176.60
38	CHA-M10	187.4	177.30	174.20	174.70

5.3 Correlation between Surface and Bulk Resistivity

The correlations of surface and bulk resistivity readings that were obtained at 28, 56, and 91 days for the moist room and SPS curing are presented in table form in Appendix A. The resistivity readings increased with time for samples cured in the moist curing room for both tests due to continued hydration and leaching. For samples cured in SPS however, any increase in time was highly dependent on the mixture type and pore solution, and will be discussed in more details in sections 5.5 and 5.6. For moist room and SPS curing. The bulk and surface resistivity measurements correlated very well with each other, as shown in Figure 5-1 and Figure 5-2.

The relationship between the surface resistivity tests for both curing methods is shown in Figure 5-3. Figure 5-4 shows the relationship between the bulk resistivity tests for both curing methods as well. Mixtures 22 and 23 containing 55% slag cement and silica fume or metakaolin showed much higher surface and bulk resistivity when cured with SPS than the trend found would have suggested, suggesting leaching in mixtures 22 and 23 when cured in the SPS. The lowest predicted pore solution conductivities for mixtures 7, 22 and 23. All three of these mixtures contained 55 or 60 percent slag cement without fly ash. Mixture 7 however was cured with a higher than predicted SPS conductivity and did not show the higher resistivity than the trend would predict with SPS curing, giving credence to this hypothesis. The bulk resistivity tests showed a better relationship between both curing methods due to less variation in the readings and issues with leaching.

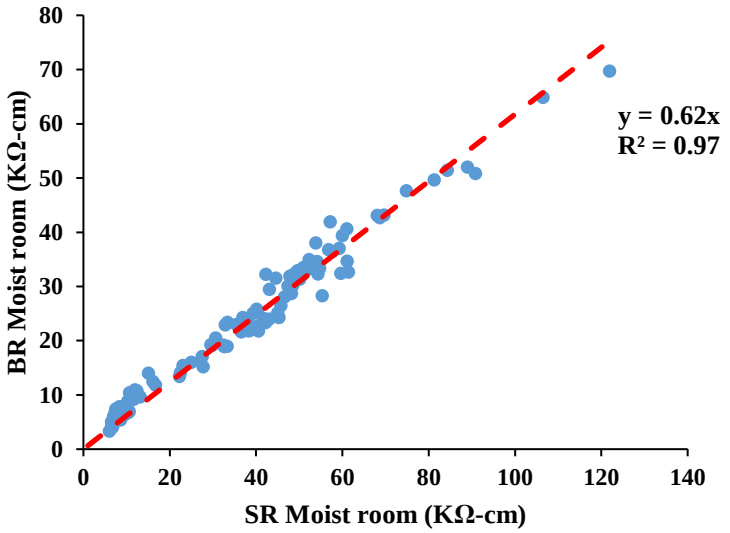

Figure 5-1: SR vs BR at all ages (moist room)

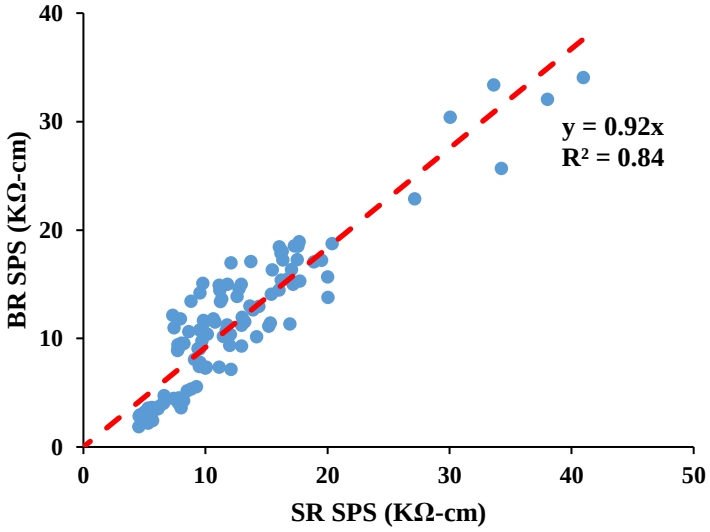

Figure 5-2: SR vs BR at all ages (SPS)

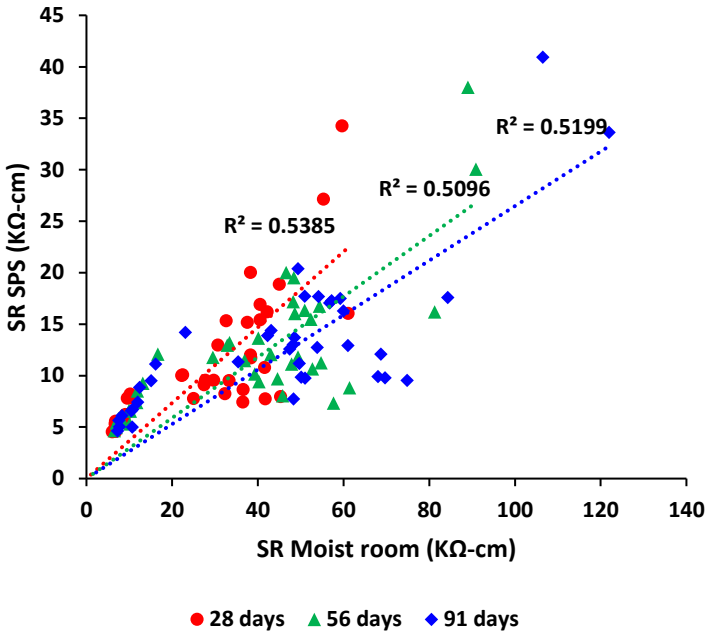

Figure 5-3: SR (moist room) vs SR (SPS) readings for all ages

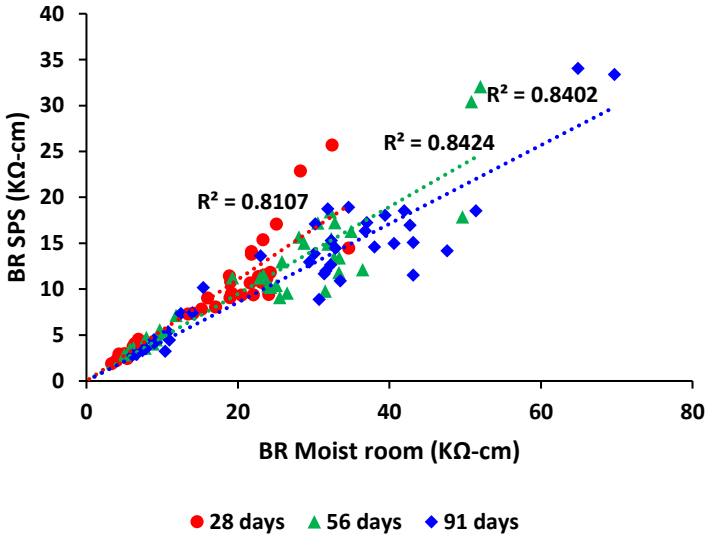

Figure 5-4: BR (moist room) vs BR (SPS) readings for all ages

5.4 Formation Factor

In this study, the formation factor was obtained from the bulk resistivity measurements and pore solution conductivity using the estimated pore solution conductivity from NIST calculator and measured SPS conductivity, assuming

equilibrium with the concrete. Table 5-2 shows the calculated formation factor for each age using the NIST calculated pore solution values for both curing methods, while Table 5-3 shows the formation factor calculated using the measured SPS conductivity values and bulk resistivity values for SPS cured samples. The mixes that were placed in the moist room exhibited a higher formation factor due to leaching impacts. Based on the results, the formation factor increases for all mixes as the time passes, and the mixes that contain 20% of fly ash and 8% of silica fume including high alkali cement (CHA-F20S8) exhibited the highest formation factor amongst the mixes performed, in which higher formation factor indicates less porous concrete and lower connectivity. The ratio of the formation factor for both different curing is 1.96 and it increases with time. Figure 5-5 shows the formation factor for all ages indicating there a good correlation between both curing methods.

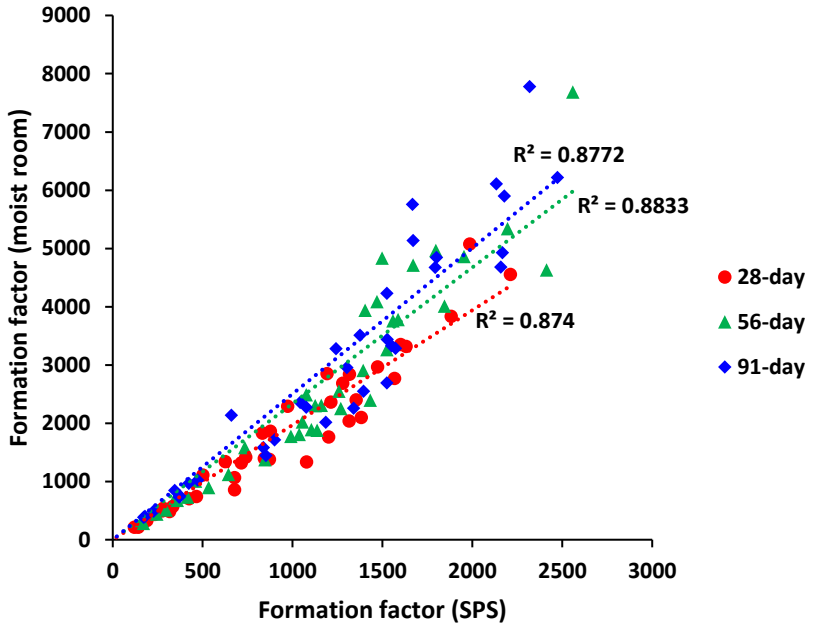

Figure 5-5: Formation factor (moist room) vs SPS curing methods

Table 5-2: Formation factor from NIST for moist curing room and SPS

Mix NO	Mix ID	NIST Calc.	Formation Factor from NIST for SPS curing			Formation Factor from NIST for moist curing room		
			28-day	56-day	91-day	28-day	56-day	91-day
1	C-100	69.6	316	359	373	480	672	750
2	C-100h	48.7	142	169	172	211	279	381
3	C-F10	115.8	466	644	851	738	1119	1444
4	C-F20	158.8	676	1136	1615	1067	1879	2445
5	C-F10h	81.8	234	297	369	433	507	728
6	C-F20h	112.9	334	534	838	568	892	1581
7	C-G60	29.9	339	516	540	680	980	1178
8	C-S8	73.7	843	1268	1394	1393	2250	2549
9	C-M10	63.2	871	991	1185	1377	1773	2014
10	C-F10G30	98.2	714	1105	1339	1319	1890	2257
11	C-F10G45	89.2	831	1160	1524	1828	2304	2693
12	C-F10G60	89.9	1382	1393	1552	2097	2904	3327
13	C-F10G60h	56.2	626	1037	1042	1339	1808	2356
14	C-F20S4	149.9	1354	1559	2167	2399	3754	4927
15	C-F20S6	145.6	1601	1953	2472	3348	4859	6219
16	C-F20S8	141.5	1280	1670	2133	2684	4714	6106
17	C-F20S8h	100.4	739	1126	1301	1418	2300	2956
18	C-F20M6	155.5	1213	1587	2157	2363	3776	4679
19	C-F20M8	154.4	1473	1403	1801	2963	3940	4845
20	C-F20M10	153.3	1632	1498	1670	3315	4834	5135
21	C-F20M10h	108.9	877	1257	1376	1860	2545	3508
22	C-G55S8	47.1	1077	1432	1572	1332	2393	3284
23	C-G55M10	26.4	678	846	899	856	1373	1713
24	CV-100	113.9	424	459	472	703	1002	1019
25	CV-100h	80.4	190	246	226	330	440	488
26	CV-F10G60	93.4	1314	1524	1526	2035	3262	3438
27	CV-F20S8	163.3	1882	2195	2318	3831	5337	7776
28	CV-M10	103.7	972	1076	1241	2288	2485	3276
29	CL-100	77.4	280	346	345	536	712	846
30	CL-100h	54.3	120	162	179	215	327	402
31	CL-F10G60	82.3	1191	1470	1524	2852	4086	4231
32	CL-F20S8	145.2	1567	2413	2177	2768	4632	5896
33	CL-M10	70.3	1200	1055	1075	1764	2019	2272
34	CHA-100	205.1	501	735	660	1110	1582	2135
35	CHA-100h	146.6	275	416	422	491	731	968
36	CHA-F10G60	122.9	1317	1845	1793	2841	4006	4672
37	CHA-F20S8	210.8	1985	2558	2430	5075	7686	9089
38	CHA-M10	187.4	2212	1796	1668	4551	4962	5756

Table 5-3: Formation factor from measured pore solution conductivity

Mix No	Mix ID	NIST Calc.	Formation Factor from measured SPS conductivity		
			28-day	56-day	91-day
1	C-100	69.6	316	358	372
2	C-100h	48.7	155	184	188
3	C-F10	115.8	297	399	522
4	C-F20	158.8	309	507	722
5	C-F10h	81.8	222	282	347
6	C-F20h	112.9	329	516	761
7	C-G60	29.9	961	1478	1532
8	C-S8	73.7	822	1218	1332
9	C-M10	63.2	851	942	1102
10	C-F10G30	98.2	709	1092	1313
11	C-F10G45	89.2	813	1133	1492
12	C-F10G60	89.9	1359	1363	1507
13	C-F10G60h	56.2	615	998	993
14	C-F20S4	149.9	1271	1450	2003
15	C-F20S6	145.6	1517	1856	2337
16	C-F20S8	141.5	1246	1616	2038
17	C-F20S8h	100.4	671	968	1071
18	C-F20M6	155.5	926	1191	1550
19	C-F20M8	154.4	1391	1322	1664
20	C-F20M10	153.3	1515	1388	1546
21	C-F20M10h	108.9	830	1071	1153
22	C-G55S8	47.1	1025	1341	1478
23	C-G55M10	26.4	696	862	926
24	CV-100	113.9	413	449	453
25	CV-100h	80.4	186	241	221
26	CV-F10G60	93.4	1295	1490	1446
27	CV-F20S8	163.3	1827	2090	2143
28	CV-M10	103.7	938	996	1101
29	CL-100	77.4	283	355	352
30	CL-100h	54.3	118	160	176
31	CL-F10G60	82.3	1171	1456	1491
32	CL-F20S8	145.2	1500	2225	2042
33	CL-M10	70.3	1175	995	1046
34	CHA-100	205.1	492	720	646
35	CHA-100h	146.6	274	410	417
36	CHA-F10G60	122.9	1298	1815	1748
37	CHA-F20S8	210.8	1811	2228	2036
38	CHA-M10	187.4	2093	1670	1555

5.5 Effect of w/cm Ratio on Surface and Bulk Resistivity

In order to study the effect of w/c ratio on the surface resistivity, some binary and ternary mixes were made with the same materials at different w/cm, 0.35 and 0.44. The surface resistivity of concrete specimens was measured at 28, 56 and 91 days for both curing environments. The surface resistivity readings for the control mixes of the four types of cement, and binary and ternary mixtures for the samples cured in the moist room is shown in Figure 5-6 Figure 5-7, respectively. As expected as the w/cm increase, the resistivity measurements decreases. For all types of cement, the resistivity increased by 20% from 28 days to 91 days, except for type 1L which only increase by 12%, indicating that the effect of limestone filler, which makes the concrete more resistant. A similar trend was seen for the sample cured in SPS as moist room curing as shown Figure 5-10 and Figure 5-11.

However, the two mixes that have 20%fly ash and 8% silica fume C-F20S8, and 20% fly ash with 10% Metakaolin C-F20M10 showed slightly showed almost no difference between the low and high w/c ratio. This might be because of alkali migration into the concrete, as the bulk resistivity measurements for C-F20S8 had higher values with the lower w/cm as expected as shown in Figure 5-11 and Figure 5-13 .The C-F20M10 had slightly higher values at the higher w/cm, but still within the range of acceptable results of multiple operators (R. P. Spragg et al., 2012). In general, for the bulk resistivity test, for the majority of the mixes, there were an increase in the resistivity over time on average of 28% for the control mixes, and 71% for the binary and ternary mixes as shown in Figure 5-12 and Figure 5-13.

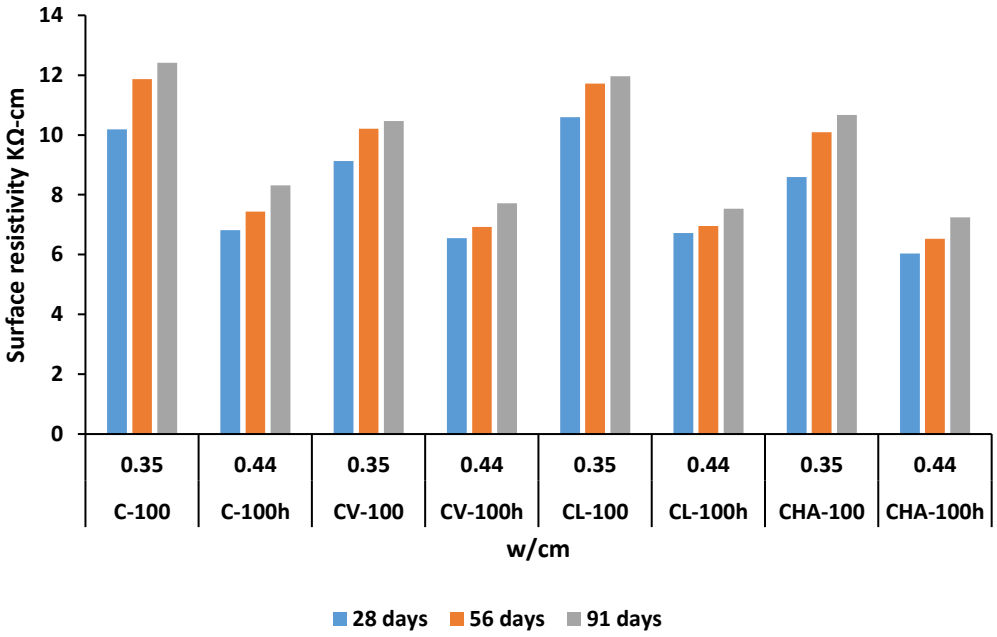

Figure 5-6: Effect of w/cm on the control mixes (moist room)

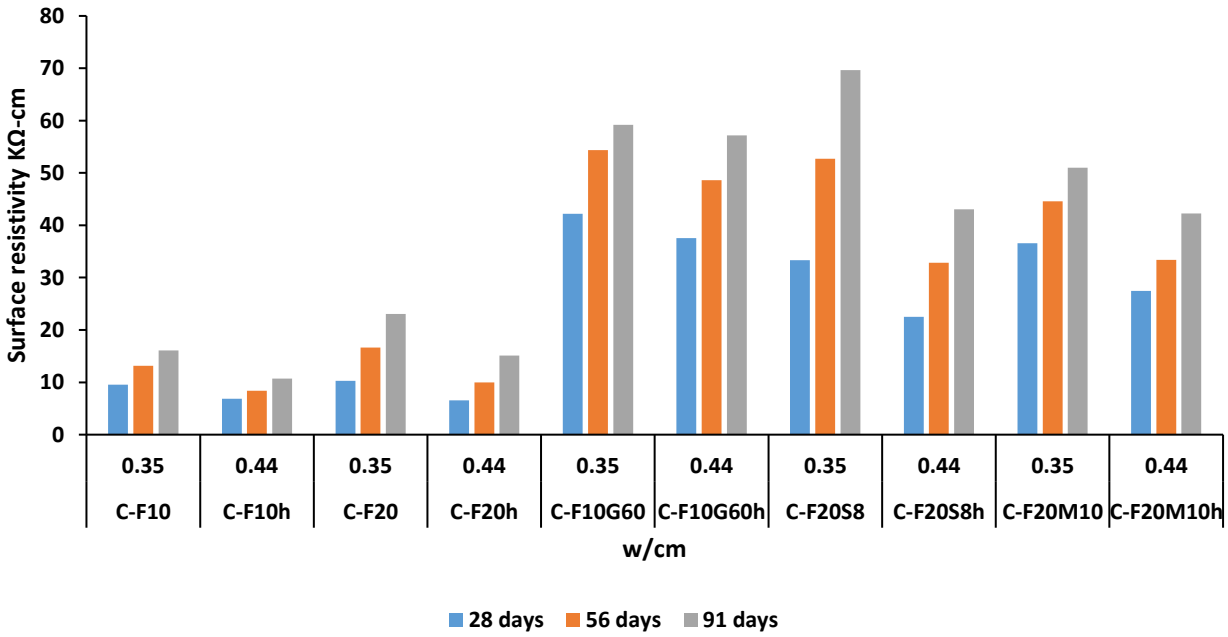

Figure 5-7: Effect of w/cm on ternary and binary mixes (moist room)

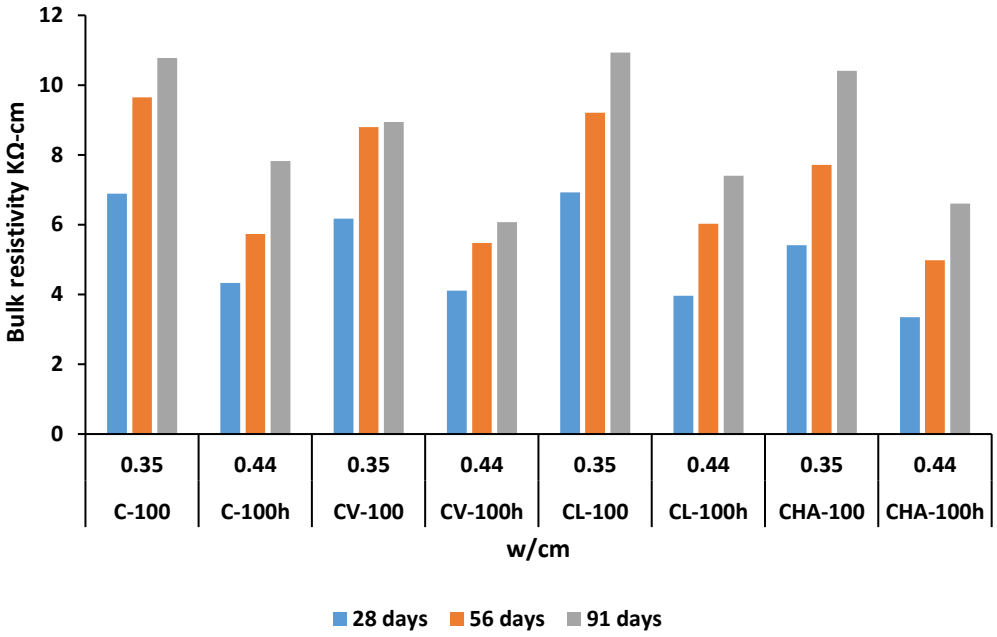

Figure 5-8: Effect of w/cm on the control mixes (moist room)

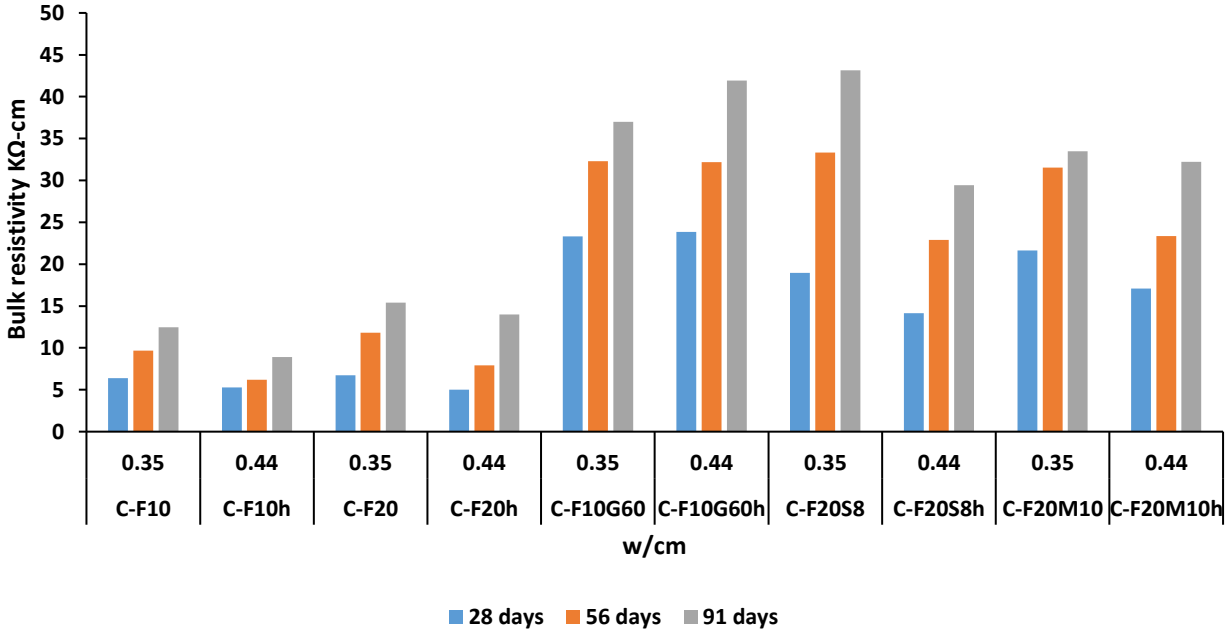

Figure 5-9: Effect of w/cm on ternary and binary mixes (moist room)

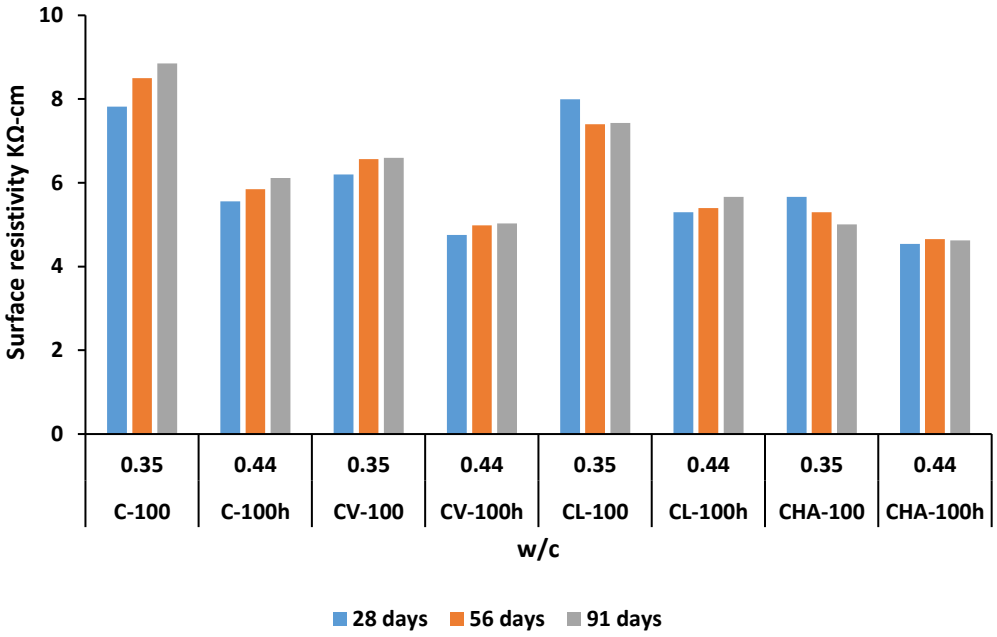

Figure 5-10: Effect of w/cm on the control mixes (SPS)

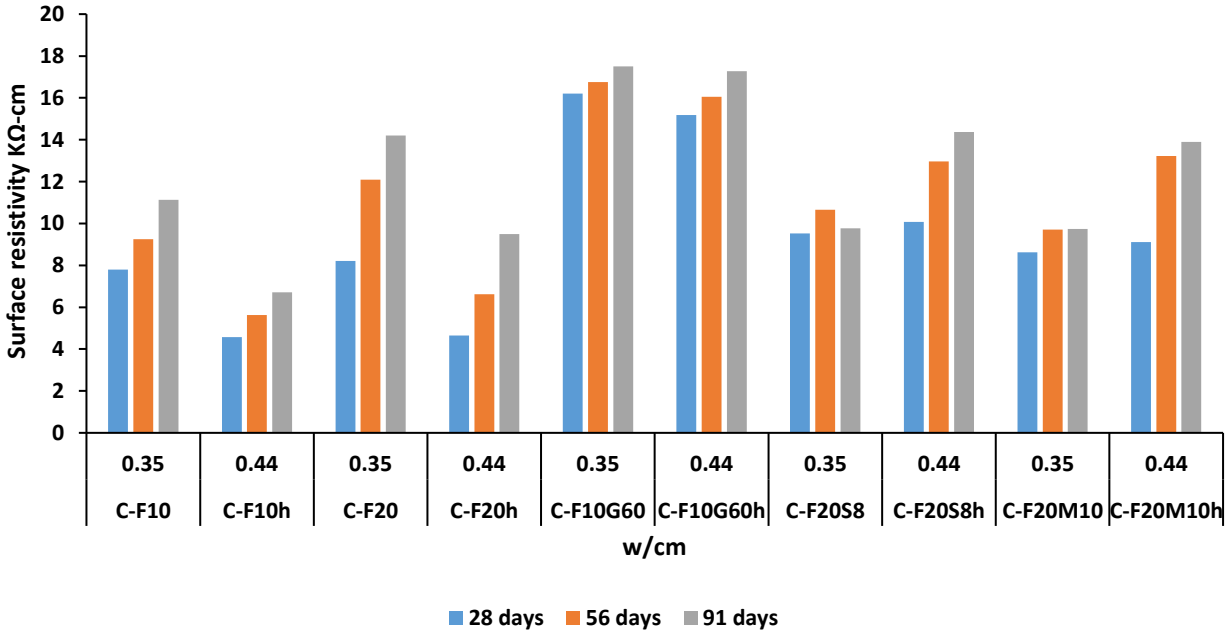

Figure 5-11: Effect of w/cm on ternary and binary mixes (SPS)

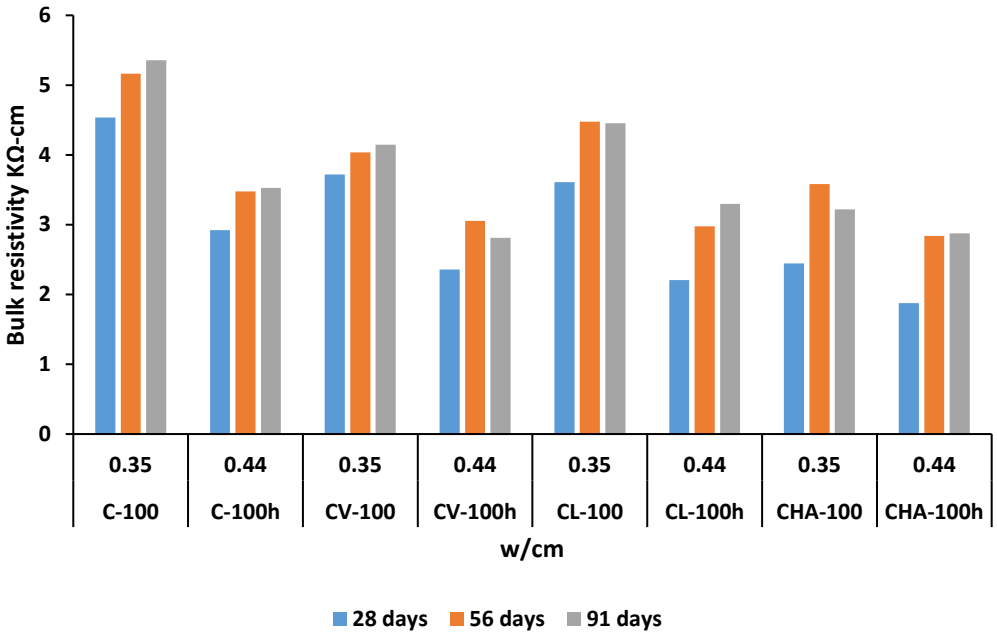

Figure 5-12: Effect of w/cm on the control mixes (SPS)

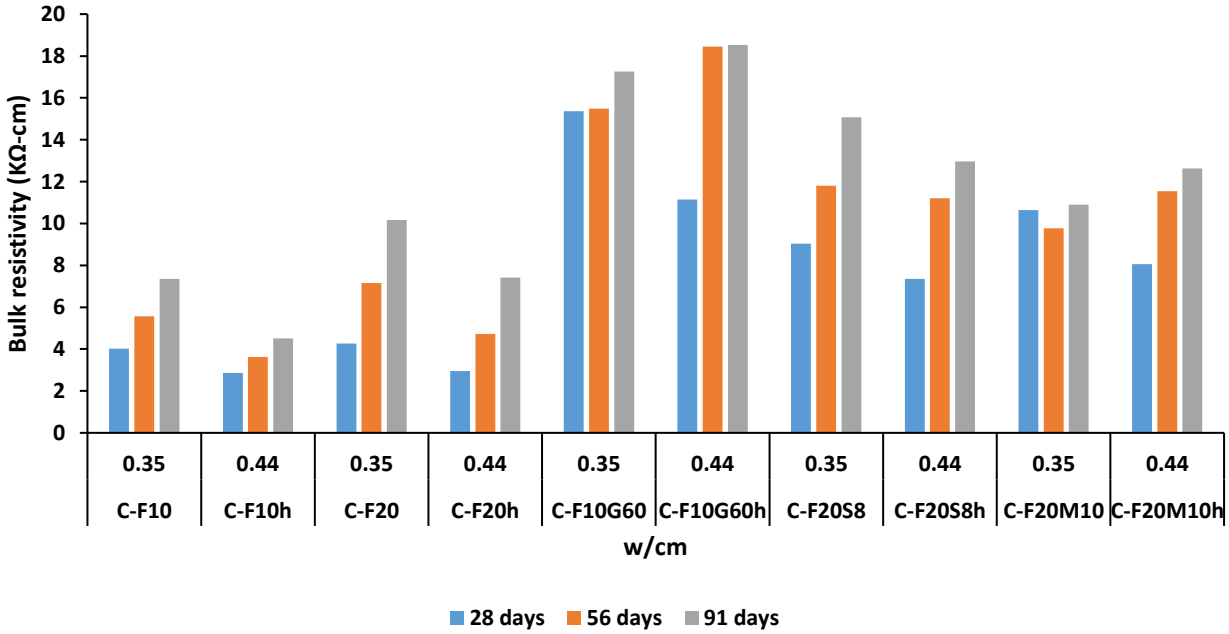

Figure 5-13: Effect of w/cm on ternary and binary mixes (SPS)

5.6 Effect of SCMs on Surface and Bulk Resistivity

In order to study the effect of SCMs including fly ash, slag, silica fume, and metakaolin on the surface and bulk resistivity tests, most of the binary and ternary mixes were performed with low w/cm (0.35) since these mixtures are typically used in extremely aggressive environments.

5.6.1 Fly Ash

The surface resistivity readings for the mixes that contain a 10% and 20% of fly ash as well as the resistivity reading for the control mix as a comparison are discussed in this section. Compared to the control mixture, the fly ash did not affect the resistivity readings at age 28 days, this is due to the slow hydration process of fly ash. However, as the percentage of fly ash increased, the resistivity increased with time.

Figure 5-14 presents also the surface resistivity readings for the moist room and SPS curing method. A similar trend was seen as the moist room for the readings here, which is that the fly ash did not affect the resistivity readings at age 28 days. With 20% fly ash, the resistivity increased by 125% in the moist room, but only 73% in SPS between 28 and 91 days. The control mixture increased by 22% from 28 to 91 days in the moist room, compared to only 13% in SPS. This suggests that 60-70% of the increases in resistivity readings typically seen with time in moist-room cured samples could be from leaching. The bulk resistivity readings for both curing is shown in Figure 5-15, which it has almost identical trend as the surface resistivity trend for both curing method. This supports that these tests correlate well with each other.

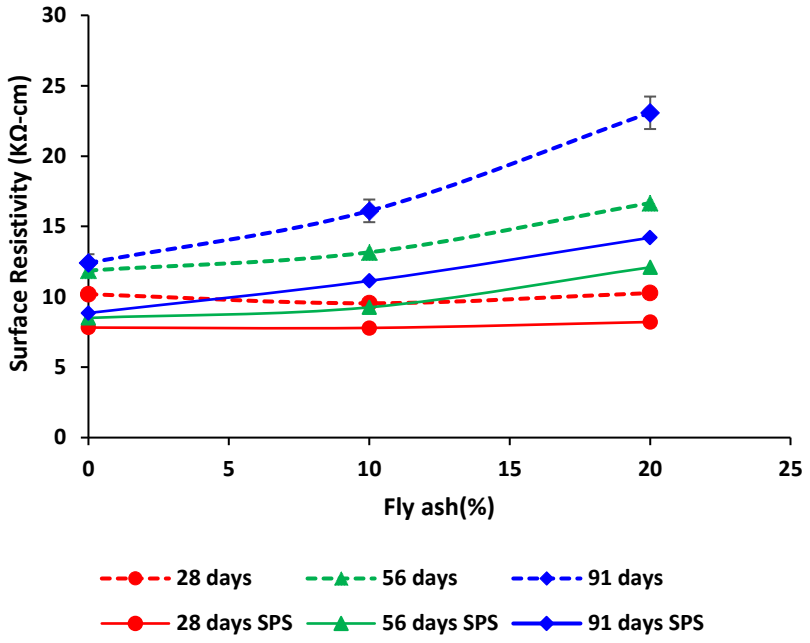

Figure 5-14: Effect of fly ash on surface resistivity readings (moist room and SPS)

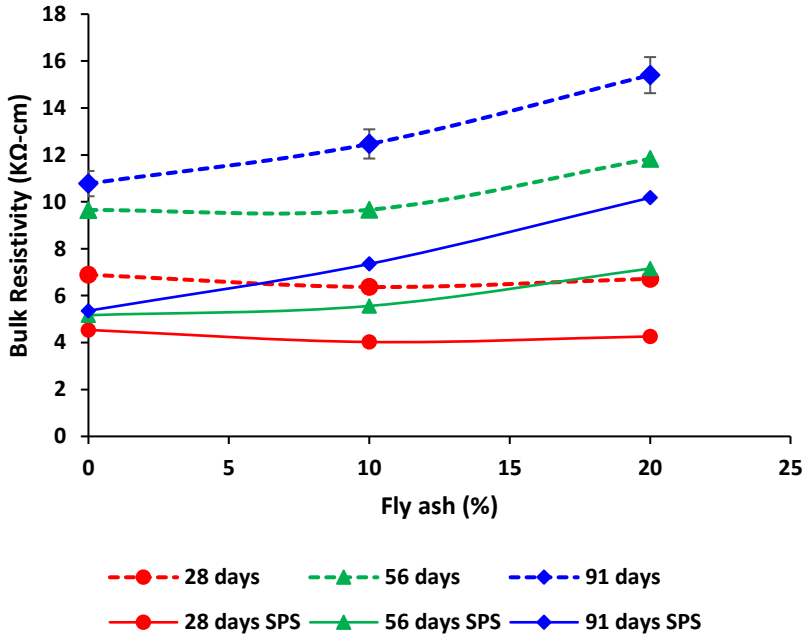

Figure 5-15: Effect of fly ash on bulk resistivity readings (moist room and SPS)

5.6.2 Slag

This section presents the surface resistivity readings for the mixes that containing a fixed 10% of fly ash, and 30%, 45% and 60% of slag as well as the resistivity reading for the control mix as a comparison. Compared to the control, as the percentage of slag increased, the resistivity increased significantly. The mixtures containing 60% slag with and without 10% fly ash showed very similar resistivity values at all ages, indicating that the fly ash had a very low degree of reaction even at 91 days, probably because of the low clinker content and calcium hydroxide consumption by the faster reacting slag mixture.

Figure 5-16 presents the surface resistivity readings for the moist room and SPS curing method. As the percentage of slag increased, the resistivity was significantly higher than control. No significant increase in surface resistivity was seen with time for the mixtures containing slag and cured in SPS, in contrast to the increase seen in bulk resistivity as shown in Figure 5-17. This could be because of the higher effect of leaching.

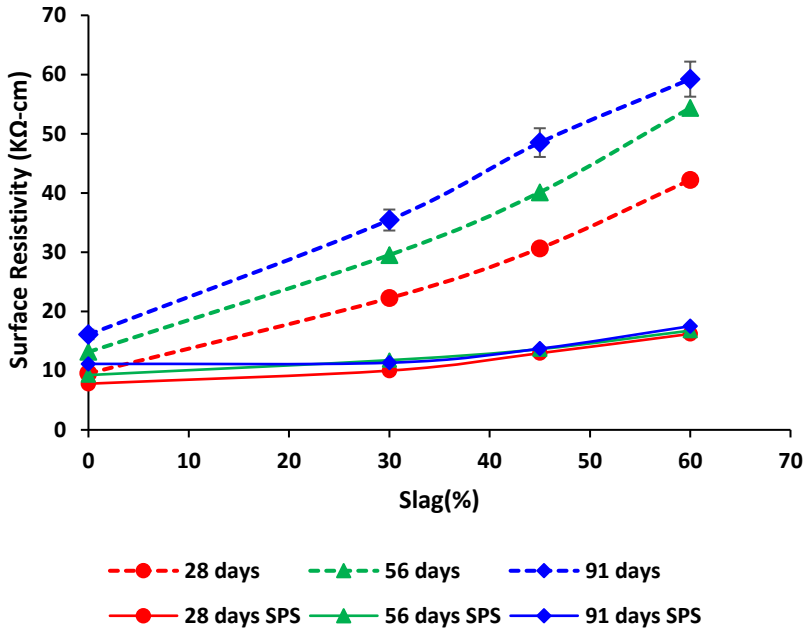

Figure 5-16: Effect of slag cement on surface resistivity readings (moist room and SPS)

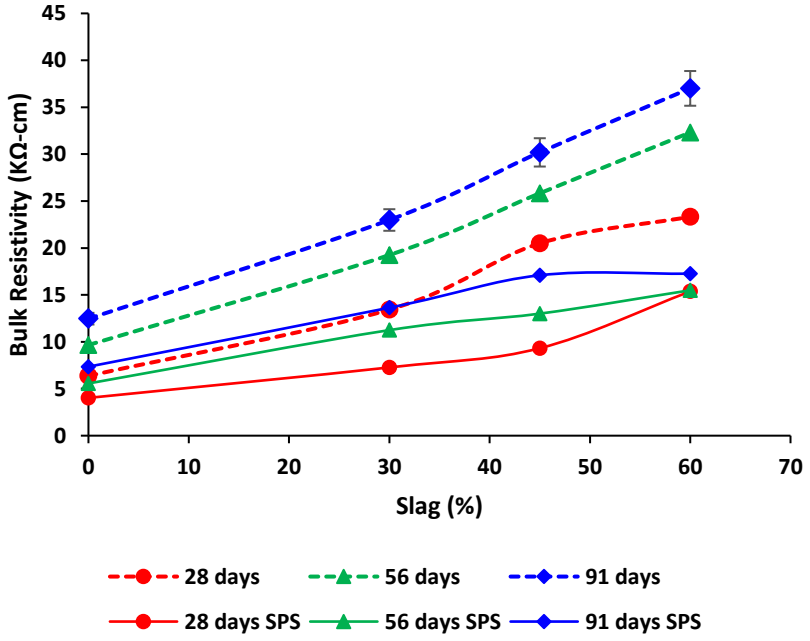

Figure 5-17: Effect of slag cement on bulk resistivity readings (moist room and SPS)

5.6.3 Silica Fume

The surface and bulk resistivity readings for the mixes that contained 20% fly ash and silica fume is shown in Figure 5-18 and Figure 5-19, respectively for samples cured

in moist room and SPS. The results showed that the use of silica fume above 6% did not further increase the surface or bulk resistivity in either curing method for ternary blends. It is possible that ternary mixtures currently being used could be economized by limiting the silica fume content, while providing similar or even improved durability.

The surface resistivity values for the mixtures containing 20% fly ash and 8% of silica fume for each of the four cements used is shown in Figure 5-20 for samples cured in the moist room and Figure 5-21 for samples cured in SPS. Similar increases in surface resistivity were seen with time for each cement used when the samples were cured in the fog room. When the samples were cured in SPS however, the little change was seen with age in the surface resistivity even though increases were seen in the bulk resistivity, as shown in Figure 5-22 and Figure 5-23. This was likely caused by alkali diffusion into the sample surface, altering the pore solution composition and reducing the surface resistivity. This illustrates the advantages of the bulk resistivity test method over the surface resistivity test method.

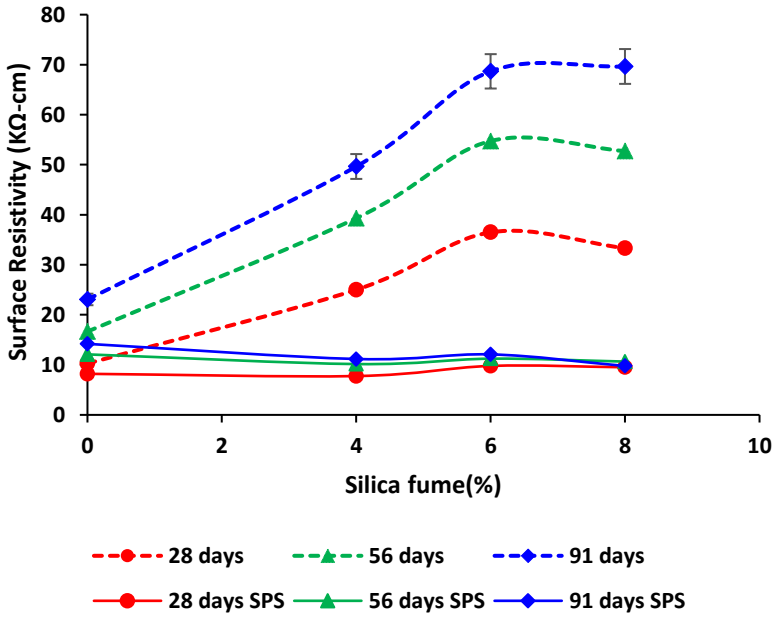

Figure 5-18: Effect of silica fume on surface resistivity readings (moist room and SPS)

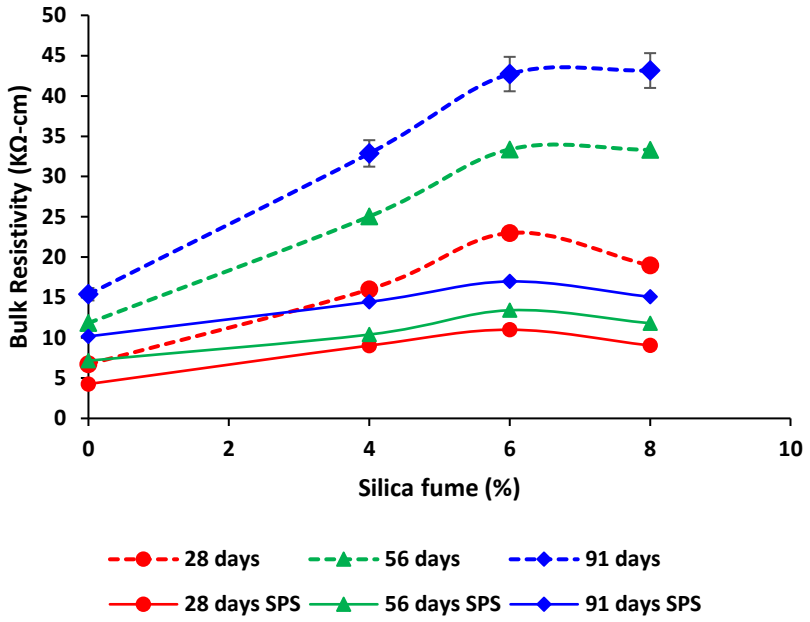

Figure 5-19: Effect of silica fume on bulk resistivity readings (moist room and SPS)

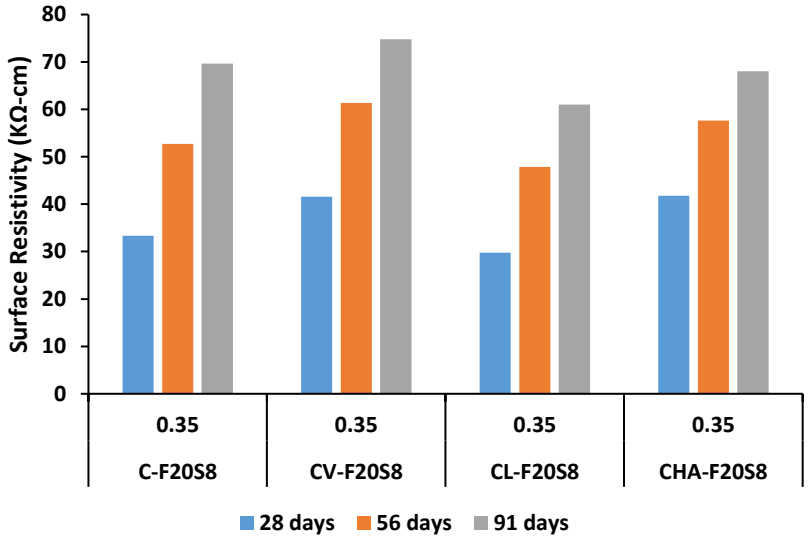

Figure 5-20: Effect of fly ash and silica fume on the different types of cement (moist room)

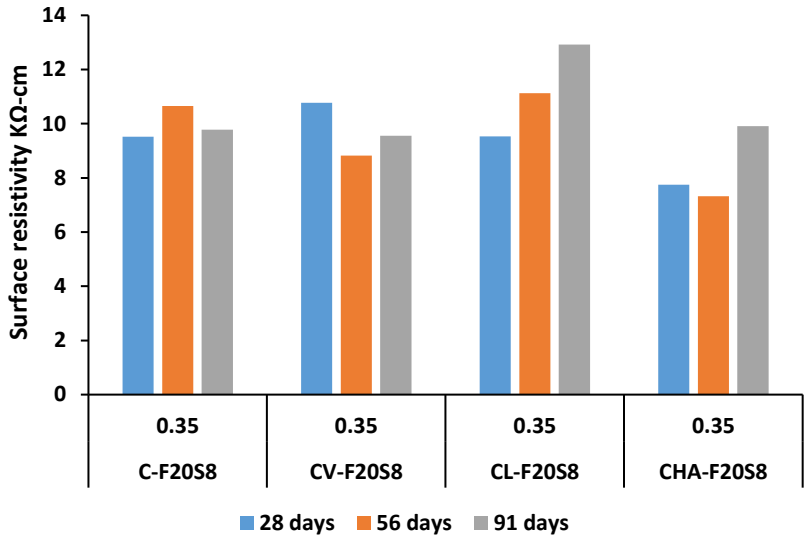

Figure 5-21: Effect of fly ash and silica fume on the different types of cement (SPS)

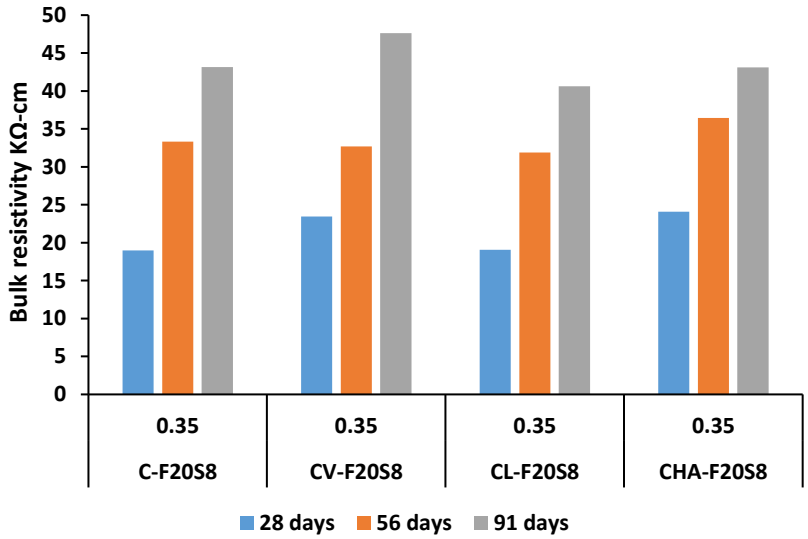

Figure 5-22: Effect of silica fume on the different types of cements (moist room)

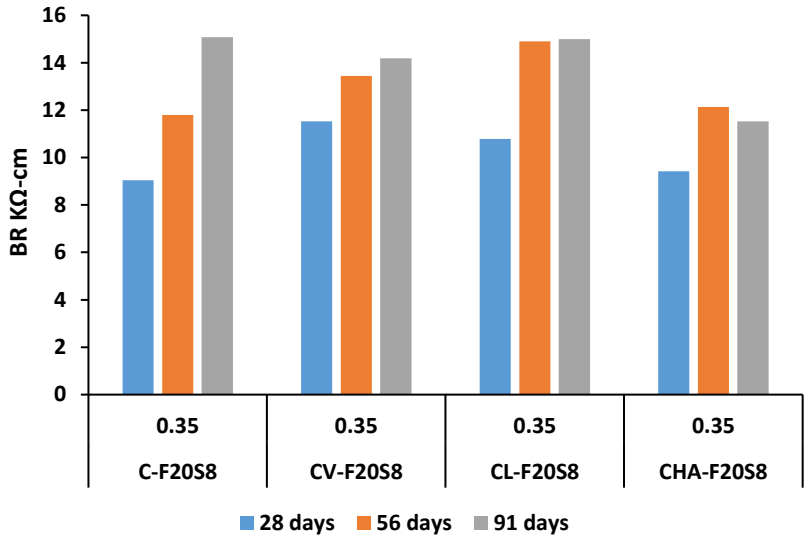

Figure 5-23: Effect of silica fume on the different types of cements (SPS)

5.6.4 Metakaolin

The surface and bulk resistivity readings for the mixes that contained 20% fly ash and 6%, 8% or 10% of metakaolin is shown in Figure 5-24 and Figure 5-25 respectively. The results reveal that the surface resistivity increased with time by 70%, 54%, and 39% for the partial replacement of cement by 6%, 8%, and 10% of metakaolin respectively. Subsequently, similar to silica fume in ternary blends, there was little long-term benefit to using more than 6% metakaolin in the concrete mixture. The metakaolin reacts faster than the fly ash, and likely consumes significant amounts of calcium hydroxide (Olufemi, 2013). The concrete likely reaches a point where the SCMs become calcium-hydroxide limited, reducing the rate of reaction and limiting the benefits of higher dosages.

A comparison of mixes that contain 10% of Metakaolin to the control mixes of the four different types of cement used is shown in Figure 5-26 and Figure 5-27 for the surface resistivity readings. For the bulk resistivity, the readings are shown in Figure 5-28

and Figure 5-29. Metakaolin provided a significant increase in the resistivity for all cements, in which it can be seen that there is no noticeable differences in the resistivity readings among the different types of cements especially for fog room curing.

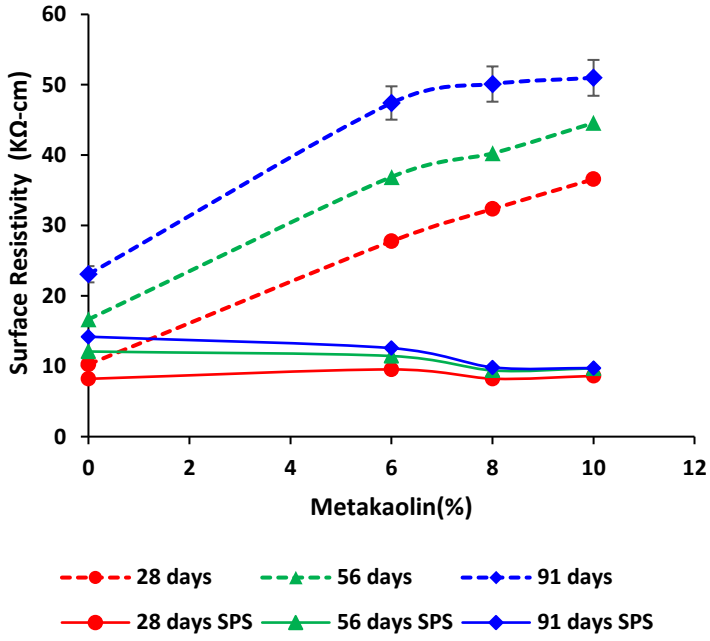

Figure 5-24: Effect of metakaolin on surface resistivity readings (moist room and SPS)

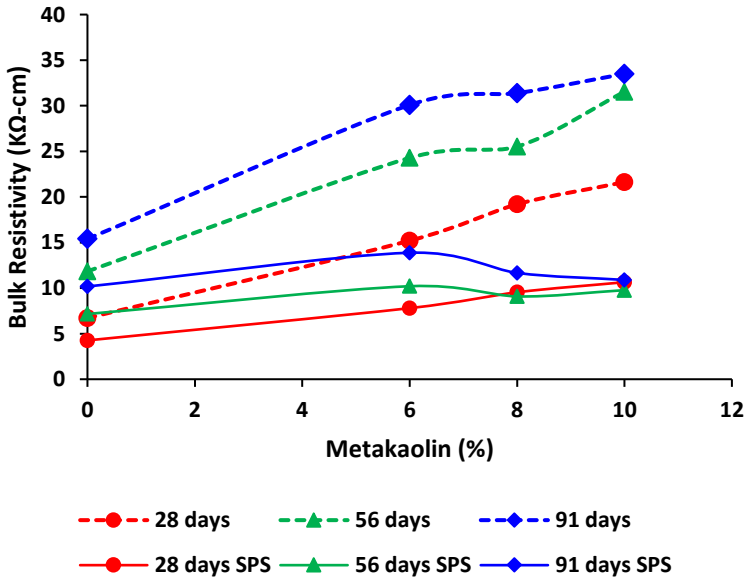

Figure 5-25: Effect of metakaolin on bulk resistivity readings (moist room and SPS)

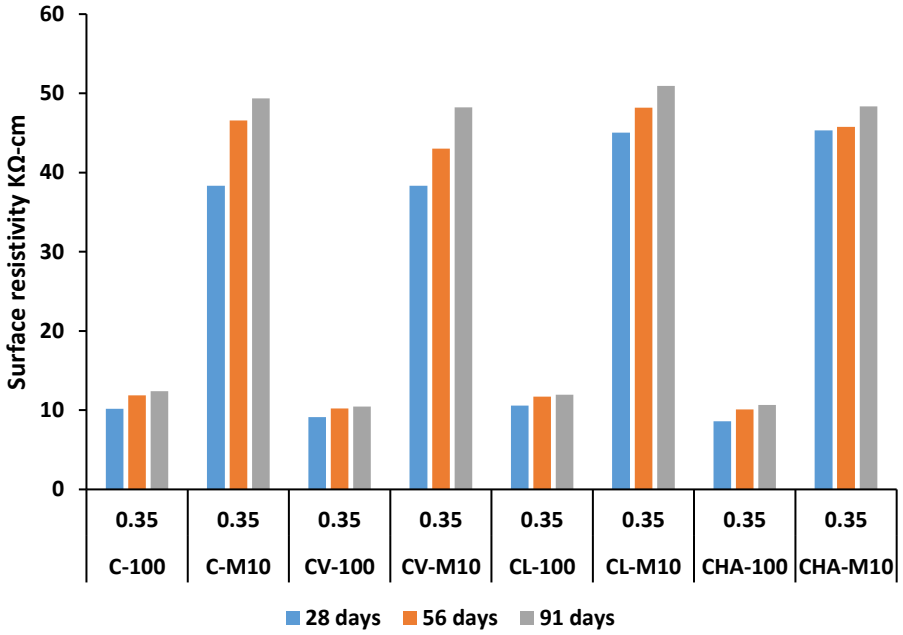

Figure 5-26: Effect of metakaolin on the control mixes (moist room)

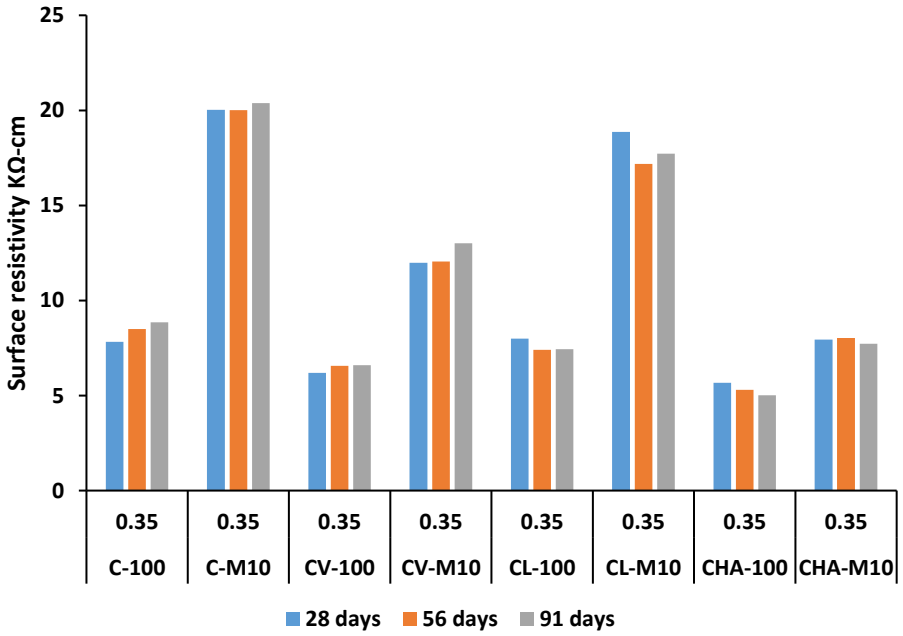

Figure 5-27: Effect of metakaolin on the control mixes (SPS)

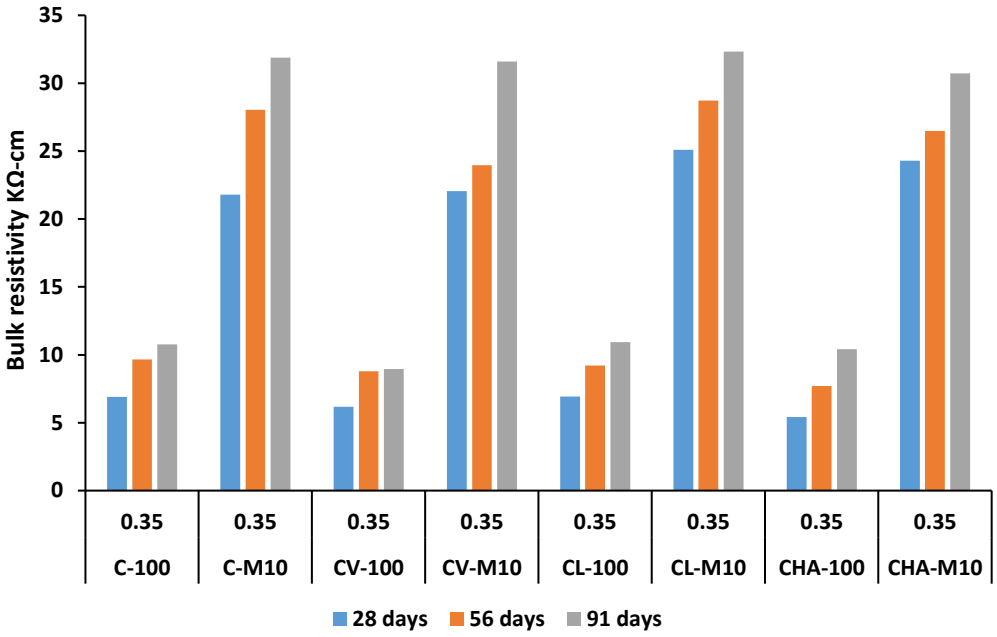

Figure 5-28: Effect of metakaolin on the control mixes (moist room)

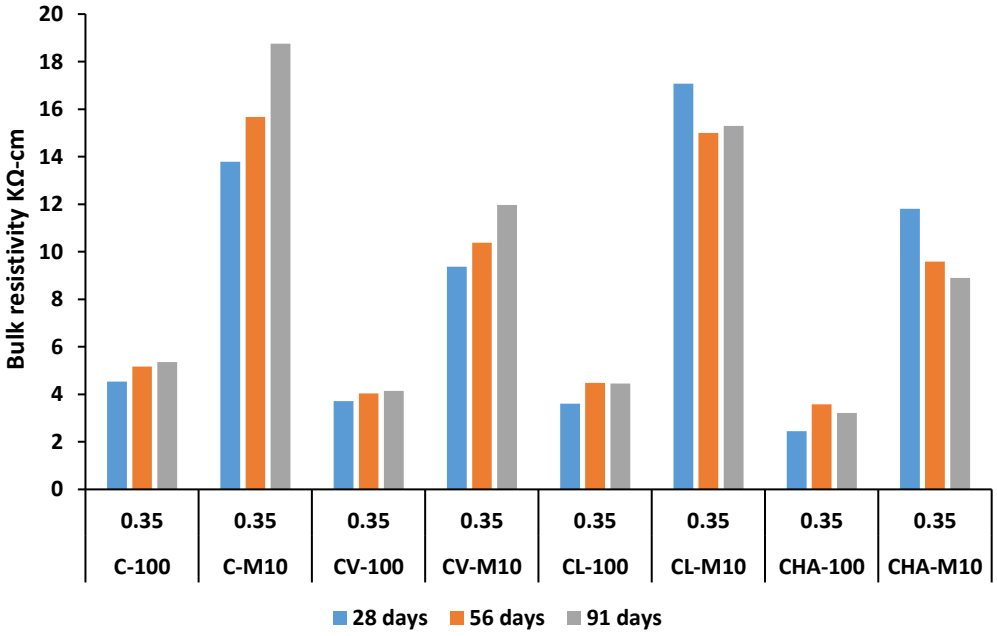

Figure 5-29: Effect of metakaolin on the control mixes (SPS)

CHAPTER 6
CONCLUSION AND FUTURE RESEARCH

6.1 Summary

Electrical measurements has become a popular method of assessing the transport properties of concrete before of their simplicity and low cost. Even though these measurements are easy to take, many factors can affect the results obtained such as: specimen geometry, temperature, pore solution, and curing methods. Therefore, samples were made from thirty-eight different concrete mixtures to determine if using a simulated pore solution to cure the concrete could give more consistent results than curing in a moist room. Based on the obtained results from this research the following conclusions can be drawn:

- Use of supplementary cementitious materials (SCMs) causes a significant increase in the surface and bulk resistivity measurements.

- As the w/cm ratio increases, the electrical resistivity decreases, which indicates less permeable and more durable concrete.

- Inconsistent resistivity results with age and SCM dosage were seen for samples cured in SPS. This is likely because of the mismatch between concrete pore solution conductivity and curing water conductivity because of errors in predicting the pore solution conductivity and changing porosity and concrete pore solution conductivity changes with continued hydration.

- There was little long-term benefit seen when the silica fume or metakaolin dosage was increased above 6% in ternary blends.

- If SPS is to be used to cure concrete samples, bulk resistivity should be used instead of surface resistivity. Surface resistivity was seen to have more issues with pore solution-curing water conductivity mismatch.

6.2 Future Research

Based on the results presented in this study, the following recommendations for future research are suggested:

- Pore solution expression is recommended to determine the validity of the NIST calculator and to determine the effects of SPS curing on the concrete pore solution.

- A correlation should be developed between the resistivity measurements and other measures of concrete transport properties such as water absorption and water permeability.

APPENDIX
SURFACE AND BULK RESISTIVITY READINGS

Table A-1. Surface and Bulk resistivity readings (moist room)

Mix #	Mix ID	W/C	SR Moist room (KΩ-cm)			BR Moist room (KΩ-cm)		
			28 days	56 days	91 days	28 days	56 days	91 days
1	C-100	0.35	10.19	11.87	12.41	6.89	9.65	10.77
2	C-100h	0.44	6.82	7.44	8.31	4.33	5.73	7.82
3	C-F10	0.35	9.54	13.16	16.11	6.37	9.66	12.47
4	C-F20	0.35	10.27	16.66	23.08	6.72	11.83	15.40
5	C-F10h	0.44	6.86	8.36	10.73	5.29	6.20	8.90
6	C-F20h	0.44	6.56	9.97	15.08	5.03	7.90	14.00
7	C-G60	0.35	40.57	50.95	59.98	22.73	32.79	39.39
8	C-S8	0.35	32.65	48.43	54.13	18.90	30.52	34.59
9	C-M10	0.35	38.33	46.59	49.35	21.80	28.05	31.87
10	C-F10G30	0.35	22.24	29.53	35.43	13.43	19.25	22.98
11	C-F10G45	0.35	30.66	40.12	48.51	20.50	25.83	30.19
12	C-F10G60	0.35	42.20	54.37	59.22	23.33	32.31	37.01
13	C-F10G60h	0.44	37.53	48.62	57.18	23.83	32.17	41.93
14	C-F20S4	0.35	25.02	39.31	49.65	16.01	25.04	32.87
15	C-F20S6	0.35	36.49	54.74	68.67	23.00	33.37	42.72
16	C-F20S8	0.35	33.33	52.73	69.64	18.97	33.31	43.15
17	C-F20S8h	0.44	22.50	32.83	43.08	14.13	22.91	29.44
18	C-F20M6	0.35	27.76	36.90	47.41	15.20	24.28	30.09
19	C-F20M8	0.35	32.34	40.25	50.10	19.19	25.51	31.38
20	C-F20M10	0.35	36.57	44.57	50.98	21.62	31.53	33.50
21	C-F20M10h	0.44	27.49	33.36	42.28	17.08	23.37	32.22
22	C-G55S8	0.35	55.32	90.88	121.91	28.28	50.81	69.72
23	C-G55M10	0.35	59.63	89.00	106.49	32.43	52.01	64.88
24	CV-100	0.35	9.13	10.21	10.47	6.17	8.79	8.95
25	CV-100h	0.44	6.55	6.93	7.72	4.11	5.48	6.07
26	CV-F10G60	0.35	40.57	52.32	56.78	21.78	34.93	36.81
27	CV-F20S8	0.35	41.59	61.37	74.79	23.46	32.68	47.62
28	CV-M10	0.35	38.35	43.00	48.24	22.06	23.96	31.59
29	CL-100	0.35	10.60	11.72	11.96	6.93	9.21	10.93
30	CL-100h	0.44	6.72	6.96	7.53	3.96	6.03	7.40
31	CL-F10G60	0.35	61.08	81.28	84.31	34.66	49.65	51.41
32	CL-F20S8	0.35	29.73	47.84	61.03	19.06	31.90	40.61
33	CL-M10	0.35	45.02	48.21	50.95	25.09	28.71	32.32
34	CHA-100	0.35	8.60	10.09	10.67	5.41	7.71	10.41
35	CHA-100h	0.44	6.04	6.53	7.25	3.35	4.99	6.60
36	CHA-F10G60	0.35	38.37	49.33	53.81	23.12	32.60	38.01
37	CHA-F20S8	0.35	41.75	57.66	68.05	24.08	36.46	43.11
38	CHA-M10	0.35	45.31	45.77	48.34	24.29	26.48	30.72

Table A-2: Surface and Bulk resistivity readings (SPS)

Mix #	Mix ID	W/C	SR SPS (KΩ-cm)			BR SPS (KΩ-cm)		
			28 days	56 days	91 days	28 days	56 days	91 days
1	C-100	0.35	7.82	8.50	8.85	4.54	5.17	5.36
2	C-100h	0.44	5.56	5.85	6.12	2.92	3.48	3.53
3	C-F10	0.35	7.79	9.25	11.13	4.02	5.56	7.35
4	C-F20	0.35	8.21	12.10	14.20	4.26	7.15	10.17
5	C-F10h	0.44	4.57	5.63	6.71	2.86	3.63	4.51
6	C-F20h	0.44	4.65	6.62	9.50	2.96	4.73	7.42
7	C-G60	0.35	16.92	16.34	16.28	11.35	17.24	18.04
8	C-S8	0.35	15.31	19.51	17.67	11.44	17.20	18.91
9	C-M10	0.35	20.03	20.01	20.39	13.79	15.68	18.75
10	C-F10G30	0.35	10.00	11.77	11.33	7.27	11.25	13.63
11	C-F10G45	0.35	12.95	13.63	13.71	9.32	13.00	17.09
12	C-F10G60	0.35	16.20	16.75	17.51	15.37	15.49	17.26
13	C-F10G60h	0.44	15.18	16.05	17.27	11.14	18.45	18.54
14	C-F20S4	0.35	7.76	10.16	11.17	9.03	10.40	14.45
15	C-F20S6	0.35	7.42	11.24	12.09	11.00	13.41	16.98
16	C-F20S8	0.35	9.52	10.65	9.78	9.04	11.80	15.08
17	C-F20S8h	0.44	10.08	12.97	14.38	7.36	11.21	12.96
18	C-F20M6	0.35	9.55	11.46	12.58	7.80	10.20	13.87
19	C-F20M8	0.35	8.23	9.40	9.85	9.54	9.08	11.66
20	C-F20M10	0.35	8.63	9.71	9.75	10.65	9.77	10.89
21	C-F20M10h	0.44	9.11	13.22	13.90	8.05	11.55	12.63
22	C-G55S8	0.35	27.15	30.04	33.62	22.87	30.41	33.37
23	C-G55M10	0.35	34.25	38.02	40.95	25.68	32.06	34.05
24	CV-100	0.35	6.20	6.57	6.60	3.72	4.03	4.15
25	CV-100h	0.44	4.76	4.98	5.03	2.36	3.05	2.81
26	CV-F10G60	0.35	15.40	15.48	17.05	14.07	16.32	16.34
27	CV-F20S8	0.35	10.77	8.83	9.55	11.52	13.44	14.19
28	CV-M10	0.35	11.98	12.05	13.00	9.37	10.38	11.97
29	CL-100	0.35	7.99	7.40	7.43	3.61	4.48	4.45
30	CL-100h	0.44	5.30	5.40	5.66	2.21	2.98	3.30
31	CL-F10G60	0.35	16.03	16.19	17.58	14.47	17.86	18.52
32	CL-F20S8	0.35	9.53	11.13	12.93	10.79	16.62	14.99
33	CL-M10	0.35	18.87	17.18	17.72	17.08	15.00	15.29
34	CHA-100	0.35	5.66	5.30	5.01	2.44	3.58	3.22
35	CHA-100h	0.44	4.54	4.65	4.63	1.88	2.84	2.88
36	CHA-F10G60	0.35	11.70	11.80	12.75	10.71	15.01	14.59
37	CHA-F20S8	0.35	7.74	7.33	9.91	9.42	12.14	11.53
38	CHA-M10	0.35	7.94	8.03	7.72	11.80	9.58	8.90

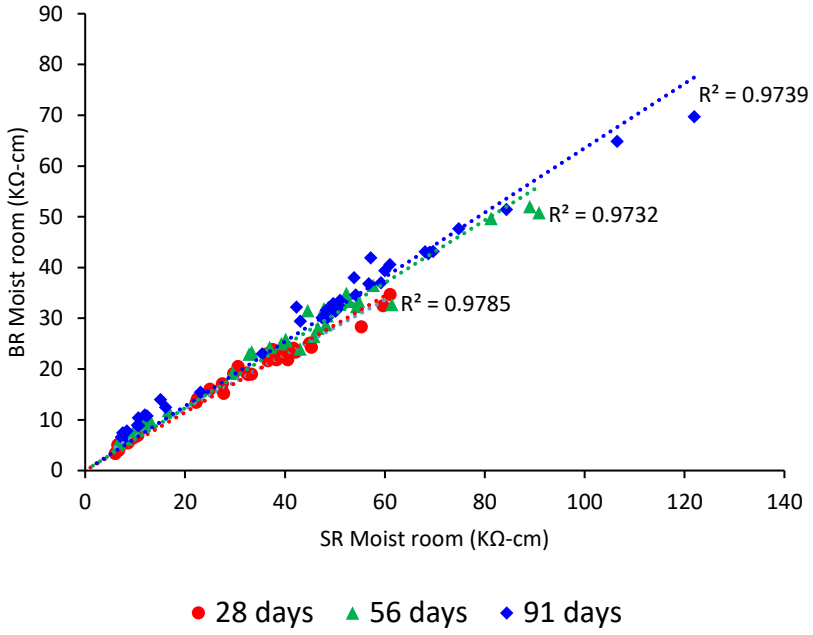

Figure A-1: Surface resistivity vs bulk resistivity (Moist room)

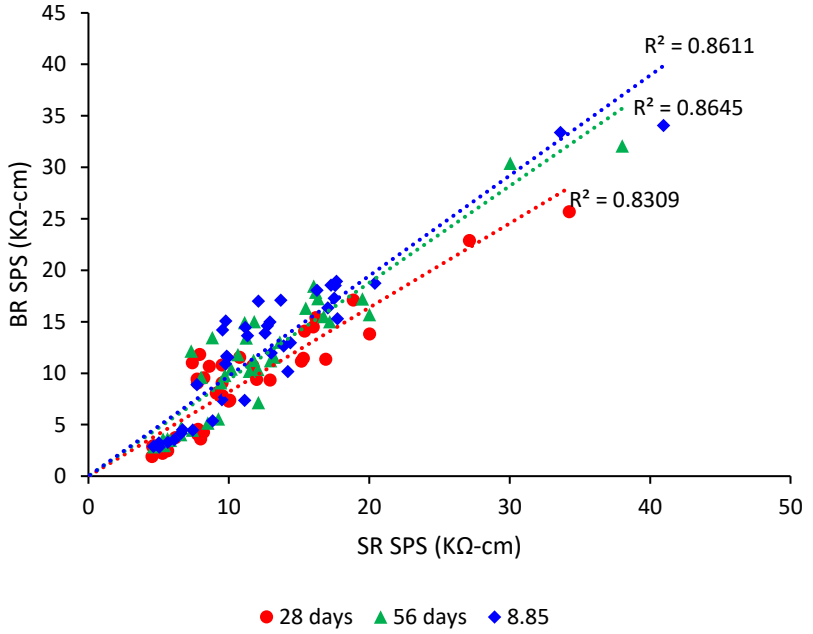

Figure A-2: Surface resistivity vs bulk resistivity (SPS

LIST OF REFERENCES

AASHTO. (2011). 95-11 Standard Method of Test for Surface Resistivity Indication of Concrete's Ability to Resist Chloride Ion Penetration. *AASHTO Provisional Standards, 2011 Edition*, 1–8. https://doi.org/10.1520/C1202-12.2

AASHTO. (2015). TP119-15 Standard Method of Test for Electrical Resistivity of a Concrete Cylinder Tested in a Uniaxial Resistance Test. *American Association of State Highway and Transportation OfficialsA*, 1–11.

ACI. (2002). Use of fly ash in concrete Reported by ACI Comittee 232. *NCHRP Synthesis of Highway Practice*, *96*(Reapproved), 1–34. Retrieved from http://trid.trb.org/view.aspx?id=277673

Ambroise, J., Maximilien, S., & Pera, J. (1994). Properties of Metakaolin blended cements. *Advanced Cement Based Materials*, *1*(4), 161–168. https://doi.org/10.1016/1065-7355(94)90007-8

Archie, G. E. (1942). The Electrical Resistivity Log as an Aid in Determining Some Reservoir Characteristics. *Transactions of the AIME*, *146*(1), 54–62. https://doi.org/10.2118/942054-G

ASTM. (2004). Standard Test Method for Temperature of Freshly Mixed Hydraulic-Cement Concrete. *Annual Book of ASTM Standards*, (c), 4–6. https://doi.org/10.1520/C1064

ASTM. (2007). Standard Specification for Portland Cement. *Annual Book of ASTM Standards*, *I*(April), 1–8. https://doi.org/10.1520/C0150

ASTM. (2010a). Standard Specification for Coal Fly Ash and Raw or Calcined Natural Pozzolan for Use. *Annual Book of ASTM Standards*, (C), 3–6. https://doi.org/10.1520/C0618

ASTM. (2010b). Standard Test Method for Air Content of Freshly Mixed Concrete by the Pressure Method. *ASTM International*, *i*, 1–10. https://doi.org/10.1520/C0231

ASTM. (2012). ASTM C1240 - 12. Standard Specification for Silica Fume Used in Cementitious Mixtures, (c), 1–7. https://doi.org/10.1520/C1240-14.2

ASTM. (2013a). Standard Specification for Slag Cement for Use in Concrete and Mortars. *ASTM Standards*, *44*(0), 1–8. https://doi.org/10.1520/C0989

ASTM. (2013b). Standard Test Method for Density (Unit Weight), Yield, and Air Content (Gravimetric). *ASTM International*, *i*, 23–26. https://doi.org/10.1520/C0138

ASTM. (2013c). Standard Test Method for Obtaining and Testing Drilled Cores and Sawed Beams of Concrete. *ASTM International*, *23*(11), 1–7.

ASTM. (2015a). C0127 - Standard Test Method for Relative Density (Specific Gravity) and Absorption of Coarse Aggregate. *ASTM International*, 5. https://doi.org/10.1520/C0127-15.2

ASTM. (2015b). Standard Test Method for Relative Density (Specific Gravity) and Absorption of Fine Aggregate. *ASTM International*, *i*, 6. https://doi.org/10.1520/C0128-15.2

ASTM. (2015c). Standard Test Method for Slump of Hydraulic-Cement Concrete. *Astm C143*, (1), 1–4. https://doi.org/10.1520/C0143

ASTM. (2016). Standard Practice for Making and Curing Concrete Test Specimens in the Laboratory. *American Society for Testing and Materials*, 1–8. https://doi.org/10.1520/C0192

ASTM. (2017). C 150/ C150M - Standard Specification for Portland Cement. *Annual Book of ASTM Standards*, 1–8. https://doi.org/10.1520/C0150

ASTM C1202. (2012). Standard Test Method for Electrical Indication of Concrete's Ability to Resist Chloride Ion Penetration. *American Society for Testing and Materials.*, (C), 1–8. https://doi.org/10.1520/C1202-12.2

Azarsa, P., & Gupta, R. (2017). Electrical resistivity of concrete for durability evaluation: A review. *Advances in Materials Science and Engineering*, *2017*. https://doi.org/10.1155/2017/8453095

Barneyback, R. S., Diamond, S., & Lafayette, W. (1981). (Communicated by D . M . Roy) (Received Nov . 21 ; in final form Dec . 29 , 1980).

Bentz, D. P. (2007). A virtual rapid chloride permeability test. *Cement and Concrete Composites*, *29*(10), 723–731. https://doi.org/10.1016/j.cemconcomp.2007.06.006

Borosnyói, A. (2016). Long term durability performance and mechanical properties of high performance concretes with combined use of supplementary cementing materials. *Construction and Building Materials*, *112*, 307–324. https://doi.org/10.1016/j.conbuildmat.2016.02.224

Bu, Y., & Weiss, J. (2014). The influence of alkali content on the electrical resistivity and transport properties of cementitious materials. *Cement and Concrete Composites*, *51*, 49–58. https://doi.org/10.1016/j.cemconcomp.2014.02.008

Bullard, JW, CF Ferraris, EJ Garboczi, NS Martys, PE Stutzman, and JE Terrill. (2008). "Chapter 10: Virtual Cement and Concrete." In Innovations in Portland Cement Manufacturing, edited by JI Bhatty, FM Miller, and SH Kosmatka, 1311–1331. Skokie, IL: Portland Cement Association.

Calleja, J. Effect of current frequency on measurement of electrical resistance of cement pastes, J. Am. Conc. Inst. 24 (1952) 329–332.

Chen, W., & Brouwers, H. J. H. (2011). A method for predicting the alkali concentrations in pore solution of hydrated slag cement paste. *Journal of Materials Science*, *46*(10), 3622–3631. https://doi.org/10.1007/s10853-011-5278-1

Cheng, A., Huang, R., Wu, J. K., & Chen, C. H. (2005). Influence of GGBS on durability and corrosion behavior of reinforced concrete. *Materials Chemistry and Physics*, *93*(2–3), 404–411. https://doi.org/10.1016/j.matchemphys.2005.03.043

Chini, A. R., Muszynski, L. C., & Hicks, J. (2003). Determination of Acceptance Permeability Characteristics for Performance-Related Specifications for Portland Cement Concrete, (July), 1–165.

Coyle, A. T., Spragg, R. P., Suraneni, P., Amirkhanian, A. N., & Weiss, W. J. (2018). Comparison of Linear Temperature Corrections and Activation Energy Temperature Corrections for Electrical Resistivity Measurements of Concrete. *Advances in Civil Engineering Materials*, *7*(1), 20170135. https://doi.org/10.1520/ACEM20170135

De La Varga, I., Spragg, R. P., Di Bella, C., Castro, J., Bentz, D. P., & Weiss, J. (2014). Fluid transport in high volume fly ash mixtures with and without internal curing. *Cement and Concrete Composites*, *45*, 102–110. https://doi.org/10.1016/j.cemconcomp.2013.09.017

Frías, M., De Rojas, M. I. S., & Cabrera, J. (2000). Effect that the pozzolanic reaction of metakaolin has on the heat evolution in metakaolin-cement mortars. *Cement and Concrete Research*, *30*(2), 209–216. https://doi.org/10.1016/S0008-8846(99)00231-8

Ganesh Babu, K., & Sree Rama Kumar, V. (2000). Efficiency of GGBS in concrete. *Cement and Concrete Research*, *30*(7), 1031–1036. https://doi.org/10.1016/S0008-8846(00)00271-4

Gowers, K. R., & Millard, S. G. (1999). Measurement of concrete resistivity for assessment of corrosion severity of steel using wenner technique. *ACI Materials Journal*, *96*(5), 536–541. https://doi.org/10.14359/655

Hadj-Sadok, A., Kenai, S., Courard, L., & Darimont, A. (2011). Microstructure and durability of mortars modified with medium active blast furnace slag. *Construction and Building Materials*, *25*(2), 1018–1025.

Hassan, Z. (2001). Binding of External Chlorides by Cement Pastes, *259*(21), 13379–13384.

Hong, S. Y., & Glasser, F. P. (1999). Alkali binding in cement pastes : Part I. The C-S-H phase. *Cement and Concrete Research*, *29*(12), 1893–1903. https://doi.org/10.1016/S0008-8846(99)00187-8

Jolicoeur, C., To, T. C., Benoît, É., Hill, R., Zhang, Z., & Pagé, M. (2009). Fly Ash-Carbon Effects on Concrete Air Entrainment : Fundamental Studies on their Origin and Chemical Mitigation. *World of Coal Ash (WOCA) Conference*, 1–23.

Joshi, P., & Chan, C. (2002). Rapid Chloride Permeability Testing. *Concrete Construction - World of Concrete*, *47*(12), 37–43.

Justice, J. M., & Kurtis, K. E. (2007). Influence of metakaolin surface area on properties of cement-based materials. *Journal of Materials in Civil Engineering*, *19*(9), 762–771. https://doi.org/10.1061/(ASCE)0899-1561(2007)19:9(762)

Kamtornkiat Musiket; Mitchell Rosendahl; and Yunping Xi. (2016). Fracture of Recycled Aggregate Concrete under High Loading Rates. *Journal of Materials in Civil Engineering*, *25*(October), 864–870. https://doi.org/10.1061/(ASCE)MT.1943-5533

Khan, S. U., Nuruddin, M. F., Ayub, T., & Shafiq, N. (2014). Effects of different mineral admixtures on the properties of fresh concrete. *TheScientificWorldJournal*, *2014*, 1–11. https://doi.org/10.1155/2014/986567

Layssi, H, et. a. (2009). Electrical Resistivity of Concrete - Time Dependence -, (October), 2–3.

Liu, Y., & Presuel-Moreno, F. J. (2014). Normalization of Temperature Effect on Concrete Resistivity by Method Using Arrhenius Law. *ACI Materials Journal*, *111*(4). https://doi.org/10.14359/51686725

Liu, Y. (2012). Accelerated curing of concrete with high volume pozzolans-resistivity, diffusivity and compressive strength [Ph.D. Dissertation], Florida Atlantic University, Boca Raton, Fla, USA.

Luo, R., Cai, Y., Wang, C., & Huang, X. (2003). Study of chloride binding and diffusion in GGBS concrete. *Cement and Concrete Research*, *33*(1), 1–7. https://doi.org/10.1016/S0008-8846(02)00712-3

Malagavelli, V. (2010b). High performance concrete, (October 2010), 591.

McCarter, W. J., Chrisp, T. M., Starrs, G., Basheer, P. A. M., & Blewett, J. (2005). Field monitoring of electrical conductivity of cover-zone concrete. *Cement and Concrete Composites*, *27*(7–8), 809–817. https://doi.org/10.1016/j.cemconcomp.2005.03.008

McCarter, W. J., Starrs, G., & Chrisp, T. M. (2000). Electrical conductivity, diffusion, and permeability of Portland cement-based mortars. *Cement and Concrete Research*, *30*(9), 1395–1400. https://doi.org/10.1016/S0008-8846(00)00281-7

Michelle, N., Adam, B., Xiaorong, W., & Douglas, H. R. (2017). Effects of Temperature , Chemical , and Mineral Admixtures, *5*(5), 1–9.

Morris, W., Moreno, E. I., & Sagüés, A. A. (1996). Practical evaluation of resistivity of concrete in test cylinders using a Wenner array probe. *Cement and Concrete Research*, *26*(12), 1779–1787. https://doi.org/10.1016/S0008-8846(96)00175-5

Neville, A. M. (2011). *Properties of Concrete*. *Journal of General Microbiology* (Vol. Fourth). https://doi.org/10.4135/9781412975704.n88

Olufemi, F. S. (2013). Reactivity of cement combinations containing Portland cement , fly ash , silica fume and metakaolin, *3*(3), 582–587.

Paredes, M., Jackson, N. M., El Safty, A., Dryden, J., Joson, J., Lerma, H., & Hersey, J. (2012). Precision Statements for the Surface Resistivity of Water Cured Concrete Cylinders in the Laboratory. *Advances in Civil Engineering Materials*, *1*(1), 104268. https://doi.org/10.1520/ACEM104268

Perraton, D. Aitcin, P., and Vezina,D. (1988). Permeabilities of Silica Fume Concrete, Am. Concr. Inst. Spec. Publ., vol. 108, pp. 63–84.

Polder, R., Andrade, C., Elsener, B., Vennesland, O., Gulikers, J., Weidert, R., & Raupach, M. (2000). RILEM TC 154-EMC : Electirical techniques for measuring-Test methods for on site measurement of resistivity of concrete. *Materials and Structures*, *33*, 603–611. https://doi.org/10.1007/BF02480599

Polder, R. B. (2001). Test methods for on site measurement of resistivity of concrete - a RILEM TC-154 technical recommendation. *Construction and Building Materials*, *15*(2–3), 125–131. https://doi.org/10.1016/S0950-0618(00)00061-1

Ponikiewski, T., & Gołaszewski, J. (2014). The effect of high-calcium fly ash on selected properties of self-compacting concrete. *Archives of Civil and Mechanical Engineering*, *14*(3), 455–465. https://doi.org/10.1016/j.acme.2013.10.014

Press, P., & May, R. (1992). SiO 2 A1203 Fe203 SO 3 MgO Na20 K20 I g n i t i o n, *22*, 15–22.

Presuel-Moreno, F., Wu, Y. Y., & Liu, Y. (2013). Effect of curing regime on concrete resistivity and aging factor over time. *Construction and Building Materials*, *48*, 874–882. https://doi.org/10.1016/j.conbuildmat.2013.07.094

Proceq SA. (2016). The world's most accurate concrete surface resistivity meter. Retrieved from https://www.proceq.com/uploads/tx_proceqproductcms/import_data/files/Resipod_Sales Flyer_English_high.pdf

Rajabipour, F., Sant, G., & Weiss, J. (2007). Development of Electrical Conductivity-Based Sensors for Health Monitoring of Concrete Materials Development of Electrical Conductivity-Based Sensors for Health Monitoring of Concrete Materials. *Transportation Research Board*, *Annual Mee*(1500), 1–16.

Ramezanianpour, A. A., & Bahrami Jovein, H. (2012). Influence of metakaolin as supplementary cementing material on strength and durability of concretes. *Construction and Building Materials*, *30*, 470–479. https://doi.org/10.1016/j.conbuildmat.2011.12.050

Riding, K. A., Poole, J. L., Schindler, A. K., Juenger, M. C. G., & Folliard, K. J. (2008). Simplified concrete resistivity and rapid chloride permeability test method. *ACI Materials Journal*, *105*(4), 390–394.

Rupnow, T., & Icenogle, P. (2011). Development of a Precision Statement for Concrete Surface Resistivity. *Transportation Research Record: Journal of the Transportation Research Board*, *2290*, 10. https://doi.org/10.3141/2290-05

Rupnow, T., & Icenogle, P. (2012). Surface Resistivity Measurements Evaluated as Alternative to Rapid Chloride Permeability Test for Quality Assurance and Acceptance. *Transportation Research Record: Journal of the Transportation Research Board*, *2290*, 30–37. https://doi.org/10.3141/2290-04

Saha, A. K. (2018). Effect of class F fly ash on the durability properties of concrete. *Sustainable Environment Research*, *28*(1), 25–31. https://doi.org/10.1016/j.serj.2017.09.001

Scott, A., & Alexander, M. G. (2016). Effect of supplementary cementitious materials (binder type) on the pore solution chemistry and the corrosion of steel in alkaline environments. *Cement and Concrete Research*, *89*, 45–55. https://doi.org/10.1016/j.cemconres.2016.08.007

Sengul, O. (2014). Use of electrical resistivity as an indicator for durability. *Construction and Building Materials*, *73*, 434–441. https://doi.org/10.1016/j.conbuildmat.2014.09.077

Sengul, O., & Gjørv, O. E. (2009). Effect of embedded steel on electrical resistivity measurements on concrete structures. *ACI Materials Journal*, *106*(1), 11–18.

Shahroodi, A. (2010). Development of Test Methods for Assessment of Concrete Durability for Use in Performance-Based Specifications Development of Test Methods for Assessment of Concrete Durability for Performance-Based Specifications.

Shane, J. D., Aldea, C. D., Bouxsein, N. F., Mason, T. O., Jennings, H. M., & Shah, S. P. (1999). Microstructural and pore solution changes induced by the rapid chloride permeability test measured by impedance spectroscopy. *Concrete Science and Engineering*, *1*(2), 110–119.

Shi, C. (2004). Effect of mixing proportions of concrete on its electrical conductivity and the rapid chloride permeability test (ASTM C1202 or ASSHTO T277) results. *Cement and Concrete Research*, *34*(3), 537–545. https://doi.org/10.1016/j.cemconres.2003.09.007

Shi, X., Xie, N., Fortune, K., & Gong, J. (2012). Durability of steel reinforced concrete in chloride environments: An overview. *Construction and Building Materials*, *30*, 125–138. https://doi.org/10.1016/j.conbuildmat.2011.12.038

Siddique, R., & Klaus, J. (2009). Influence of metakaolin on the properties of mortar and concrete: A review. *Applied Clay Science*, *43*(3–4), 392–400. https://doi.org/10.1016/j.clay.2008.11.007

Silva, A. S., Ribeiro, A. B., Jalali, S., & Divet, L. (2015). The Use of Fly Ash and Metakaolin for the Prevention of Alkali-Silica Reaction and Delayed Ettringite Formation in Concrete.

Snyder, K. A. (2001). The relationship between the formation factor and the diffusion coefficient of porous materials saturated with concentrated electrolytes: Theoretical and experimental considerations. *Concrete Science and Engineering*, *3*(9), 216–224. https://doi.org/10.1017/CBO9781107415324.004

Snyder, K. A., Ferraris, C., Martys, N. S., & Garboczi, E. J. (2000). Using Impedance Spectroscopy to Assess the Viability of the Rapid Chloride Test for Determining Concrete Conductivity. *Journal of Research of the National Institute of Standards and Technology*, *105*(4), 497–509. https://doi.org/10.6028/jres.105.040

Sohn, D., & Mason, T. O. (1998). Electrically induced microstructural changes in portland cement pastes. *Advanced Cement Based Materials*, *7*(3–4), 81–85. https://doi.org/10.1016/S1065-7355(97)00056-4

Song, H. W., Pack, S. W., Nam, S. H., Jang, J. C., & Saraswathy, V. (2010). Estimation of the permeability of silica fume cement concrete. *Construction and Building Materials*, *24*(3), 315–321. https://doi.org/10.1016/j.conbuildmat.2009.08.033

Spragg, R., Bu, Y., Snyder, K., Bentz, D., & Weiss, J. (2013). Electrical Testing of Cement-Based Materials: Role of Testing Techniques, Sample Conditioning. https://doi.org/10.5703/1288284315230

Spragg, R. P., Castro, J., Nantung, T., Paredes, M., & Weiss, J. (2012). Variability Analysis of the Bulk Resistivity Measured Using Concrete Cylinders. *Advances in Civil Engineering Materials*, *1*(1), 104596. https://doi.org/10.1520/ACEM104596

Spragg, R., Villani, C., Snyder, K., Bentz, D., Bullard, J., & Weiss, J. (2013). Factors That Influence Electrical Resistivity Measurements in Cementitious Systems. *Transportation Research Record: Journal of the Transportation Research Board*, *2342*(2342), 90–98. https://doi.org/10.3141/2342-11

Su, J., Yang, C., Wu, W., and Huang, R. (2002). Effect ofmoisture content on concrete resistivity measurement," Journal of the Chinese Institute of Engineers, vol. 25, no. 1, pp. 117–122.

Thomas, M. D. A., Hooton, R. D., Scott, A., & Zibara, H. (2012). The effect of supplementary cementitious materials on chloride binding in hardened cement paste. *Cement and Concrete Research*, *42*(1), 1–7. https://doi.org/10.1016/j.cemconres.2011.01.001

Thomas, M., Fournier, B., & Folliard, K. (2006). Test Methods for Evaluating Preventive Measures for Controlling Expansion due to Alkali-Silica Reaction in Concrete. *University of Taxes*, 62.

Van Noort, R., Hunger, M., & Spiesz, P. (2016). Long-term chloride migration coefficient in slag cement-based concrete and resistivity as an alternative test method. *Construction and Building Materials*, *115*, 746–759. https://doi.org/10.1016/j.conbuildmat.2016.04.054

Villagrán Zaccardi, Y. A., García, J. F., Huélamo, P., & Di Maio, Á. A. (2009). Influence of temperature and humidity on Portland cement mortar resistivity monitored with inner sensors. *Materials and Corrosion*, *60*(4), 294–299. https://doi.org/10.1002/maco.200805075

Vollpracht, A., Lothenbach, B., Snellings, R., & Haufe, J. (2016). The pore solution of blended cements: a review. *Materials and Structures/Materiaux et Constructions*, *49*(8), 3341–3367. https://doi.org/10.1617/s11527-015-0724-1

Vuk, T., Tinta, V., Gabrovšek, R., & Kaučič, V. (2001). The effects of limestone addition, clinker type and fineness on properties of Portland cement. *Cement and Concrete Research*, *31*(1), 135–139. https://doi.org/10.1016/S0008-8846(00)00427-0

Wainwright, P. J., & Rey, N. (2000). Wainwright, P.,and Rey, N., " The influence of ground granulated blastfurnace slag (GGBS) additions and time delay on the bleeding of concrete". Cement and Concrete Composites, 22(4), pp.253-257, 2000., *22*, 253–257. https://doi.org/10.1017/CBO9781107415324.004

Weiss, J., Snyder, K., Bullard, J., & Bentz, D. (2012). Using a Saturation Function to Interpret the Electrical Properties of Partially Saturated Concrete. *Journal of Materials in Civil Engineering*, *25*(8), 1097–1106. https://doi.org/10.1061/(ASCE)MT.1943-5533.0000549

Weiss, W., Shane, J., Mieses, A., Mason, T., Shah, S.(1999). Aspects of monitoring moisture changes using electrical impedance spectroscopy, in: Second Symposium on the Importance of Self Desiccation in Concrete Technology,Lund, Sweden.

Wenner, F. (1916). A method of measuring earth resistivity. *Bulletin of the Bureau of Standards*, *12*(4), 469. https://doi.org/10.6028/bulletin.282

Xu, Y. (1997). The influence of sulphates on chloride binding and pore solution chemistry. *Cement and Concrete Research*, *27*(12), 1841–1850. https://doi.org/10.1016/S0008-8846(97)00196-8

Yamei, Z., Wei, S., & Lianfei, S. (1997). Mechanical Properties of High Performance Concrete Made With High Calcium High Sulfate Fly Ash. *Cement and Concrete Research*, *27*(7), 1093–1098. https://doi.org/10.1016/S0008-8846(97)00087-2

BIOGRAPHICAL SKETCH

Raid Alrashidi was born in Hail, Saudi Arabia, in 1991. In 2009, he started his career at University of Hail, where he received the degree of Bachelor of Science in civil engineering in 2014. After that, he worked as a civil engineer at Saudi Oger Company for a year and half. He then enrolled in graduate school at the University of Florida where he received a Master of Science in civil engineering in August 2018. His research interests include durability of concrete structures.